Firestone Tire Failure Analysis

Dr. Sanjay Govindjee

January 30, 2001

1 Abstract

This report is an assessment of what is presently understood about the recent Firestone ATX and AT tire problems. It provides an overview of factors related to tire failures of the type observed. Example computations are presented that indicate the relative importance of a selection of variables on crack tip driving forces. An assessment of experimental data collected by Bridgestone/Firestone laboratories and an independent testing lab on returned tires is also given. The report concludes with summary observations based upon more detailed statements made within the body of the report.

The problem of belt separation is understood to be the propagation of a fatigue crack in the bulk of the rubber separating the two steel belts of the tire, not at the interface between the steel and the rubber. The important factors for this type of failure are the capacity of the material to resist the propagation of the crack and the forces that are driving the crack forward. An understanding of the problem is complicated by the fact that there are no well established criteria for in-service tire failures against which tire components are designed. Secondly, analytical techniques for predicting failures such as belt separations are only today becoming technically feasible. Thus while one can and does perform many standard laboratory tests on tires and their components it is not clear how these are related to in-service failures.

A survey of material properties from returned tires shows that materials from tires in southern climates have reduced ductility (extensibility) and higher stiffness. These observations are interestingly independent of service condition. Further, the capacity of the belt skim rubber to resist catastrophic fracture is markedly reduced for tires that were manufactured in Decatur versus those manufactured in Wilson or Joliette. This reduced fracture resistance is present in brand new tires, fresh plant stocks, unworn tires, and used tires. The weakness of the inter-belt materials shows even without service or thermal aging. Aging, however, does contribute to additional degradation. In this regard, heat build-up from low inflation pressure, heavy vehicle loads, and high speeds is detrimental to the structural integrity of the tires. A search for the causative agent for these plant differences centered around Decatur's pelletizing material mixing stages and in particular focused upon differences in material additives. This search, however, did not lead to the discovery of a causative agent for the degraded material properties from the Decatur plant.

Lacking established standards for the relevant material properties, state-

of-the-art finite element computations were performed to help understand the problem at hand. The theoretical energy release rates for these tires place the crack growth rates in the sub-nanometer per tire revolution range. Of the factors of inflation pressure, speed, vehicle load, and belt design, vehicle load plays the most important role in controlling crack growth rates. The other factors certainly play a role, but for the cases examined, vehicle load always dominated.

Overall, it is noted that the problem at hand is rather complex, the failure rates are fractions of a percent, and thus determining a single cause for the tire failures is an unrealistic expectation.

Contents

List of Figures

List of Tables

2 Introduction

2.1 Scope

The recent failures of Firestone ATX and AT tires used upon Ford Explorers was the impetus for the preparation of this report. The scope of the report is limited to an examination of the performance of the tires when used upon Ford Explorers. Other issues of interest related to the details of vehicle roll-over are not covered by this study. The primary goal of the report is to examine the presently available physical and theoretical facts concerning the tires and make where warranted appropriate inferences and conclusions.

2.2 Basic phenomenon

An examination of tires that have been submitted to Firestone from accidents involving Ford Explorers shows that the basic failure of the tire is a belt separation between the #1 and #2 steel belts. A visual examination of the failure surfaces reveals two regimes of crack growth: (1) a large region where the material has torn as part of the final event of belt separation, and (2) a smaller region closer to the #2 belt edge which is smooth and polished. The presence of this second region supports the conjecture of a slow growing fatigue crack in the tire. The polished appearance is the result of the rubbing of the crack faces each time they pass through the footprint[1]. Unfortunately, the polishing action erases the fatigue striations which are normally utilized in identifying and understanding such failures. It is to be noted that belt edge cracks are common to steel belted radial tires due to the large stress concentration that is present at the belt edge from the material stiffness discontinuity between the steel and rubber; shown in Fig. 1 is an example of a belt edge crack from a passenger tire that developed in a laboratory experiment.

2.3 Problem frequency

The failures that are to be investigated are low frequency occurrences. The number of lawsuit claims that have been filed represent a very small fraction of the number of tires produced. Perhaps a more important database for

---

[1]The hypothesis of closed crack rubbing is supported by finite element analysis.

understanding the number of units that are failing is the warranty adjustments data which represents tires that have been deemed defective in some fashion after use. The usefulness of this database is that it contains many more data points and is thus statistically more significant. An examination of this database shows that warranty claims that are associated with either the tread or the belt occur at a rate of a small fraction of a percent when looking at all passenger tires produced by Firestone over the last 10 years[2]. For the ATX tire over this same period the adjustment rate for Decatur produced tires was 4.6 times the base rate, for Joliette produced tires it was 1.9 times the base rate, and for Wilson produced tires it was 2.8 times the base rate. These rates are certainly above the base rate for Firestone's passenger tires but as absolute numbers (fractions of a percent) they are still small within the context of trying to determine causative factors. A similar statement can be made when looking at the Wilderness AT. This tire has only been in production since 1996. For Firestone passenger tires produced in 1996-1999 the adjustment rate was 0.5 times the base rate. For the Wilderness AT tires made in Decatur over this period the adjustment rate was 0.8 times the base rate, for tires produced in Wilson it was 0.7 times the base rate, and for tires produced in Joliette it was 0.8 times the base rate. As an additional point of comparison, the ATX tire over this production period had for Decatur produced tires an adjustment rate 4.1 times the base rate, for Joliette produced tires an adjustment rate 1.3 times the base rate, and for Wilson produced tires an adjustment rate 2.7 times the base rate. In all cases, failure rates are fractions of a percent and thus determining a single cause for the tire failures is an unrealistic expectation. Such a determination is further complicated by the present state of tire technology which does not present well established failure criteria for tires.

2.4 Important factors

Determining the causative factors of belt separation revolves about two different issues: (1) what is the capacity of the material to resist the propagation of cracks, (2) what is the demand or force that is driving the crack forward.

Capacity in this context is composed of two sets of material properties:

1. The critical energy release rate for the material.

---

[2]The precise value of this fraction is considered company confidential data and is thus not reported here. In what follows this value is referred to as the *base rate*.

2. The fatigue growth properties.

The first of these material properties governs when the crack will propagate catastrophically. The second set of properties govern how the crack evolves before the catastrophic event. It is noted that both sets of properties are affected by material history – most notably by thermal aging. Here and throughout "material properties" is taken to refer to both bulk and interfacial properties.

Demand in the present context is composed of several points:

1. Forces and moments the vehicle delivers to the tire.

2. Inertial forces from tire rotation.

3. Thermal load on the tire.

The first two of these factors influence the crack tip driving forces (energy release rates) and their importance needs to be determined; this determination naturally depends on the particular tire design in question. The primary effect of the third point is to negatively influence material capacity.

2.5   Capacity

The most direct method to determine the capacity of the materials is to test them in the laboratory. In this context there are two materials that need to be examined, the rubber that encases the steel belts which is known as the belt skim and the material that is placed between the #2 belt edge and the #1 belt and is known as the wedge. In the AT and ATX tires the belt skim is a natural rubber compound known as J2757 and the wedge material is a natural rubber compound known as J2917. In March of 1998 the wedge material was changed to J2757. It is noted that due to differences in the plant processing methods employed, not all plants produce exactly the same compounds and this needs to be taken into account in test design. In the report to follow, the capacity of the materials is tested in two ways. First, the capacity is measured by extracting material samples from actual tires that were collected during the recall and then testing them in the laboratory. Second, new batches of materials were made in the laboratory and then tested using standard lab tests. In doing this second set of tests, the issue of material aging was addressed by accelerated aging in an oxygen environment at elevated temperatures (100C for 2 days). It is noted that the use of an O_2

environment may emphasize the role of the oxidative aspects of aging over those associated with cross-link re-arrangement. The choice of 100C for 2 days is partially justified by the experimental observation that after 2 days at 100C the properties of elongation to break, 100% modulus, and tensile stress at break from accelerated aging bound 9 year field data for these materials.

2.6   Demands

The demands placed on the tire were determined by field testing of vehicles on test tracks. The temperature of the belt region of the tire was determined at several speeds, a range of inflation pressures, and at two different cargo loads. The forces and moments the vehicle delivered to the tires were measured using static weigh scales and dynamic load cells placed between the vehicle and tire. These measurements were performed at four different inflation pressures, four different cargo loads, and at several different vehicle speeds. The inertial forces were not directly measured and were computed from basic principles of physics. The conversion of the force and moment data to crack tip energy release rates was made using finite element analysis; these computations were performed using state-of-the-art methods based upon research which is presently in press [65]. The variation of crack tip energy release rates with respect to design variations has only been examined for changes in steel cord end-count and belt angle.

2.7   Overview

The organization of the remainder of this report is as follows. First, a presentation is given of the data collected from the demand measurements and results of finite element computations to estimate energy release rates. Next there is a presentation of the data collected from returned tires. This is followed by data from standard laboratory tests. The report closes with a summary of what can be reasonably concluded from what is presently known. Figures, tables, and a brief glossary may be found at the end of the report.

3   Tire demands

Tire demands that are of importance in the present context consist of thermal load and mechanical load. Thermal load is important in that it is well

known that elastomer properties are affected by temperature. This appears as a dependency upon the thermal history and a dependency upon the present temperature. The history dependence is mainly associated with permanent degradation (or aging) at elevated temperatures. The primary physical mechanisms are commonly thought to be crosslink evolution, chain scission, and compound component migration. The literature in this area is very extensive and includes many theoretical models and much experimental work; for a small sampling of the available literature see e.g. [62, 68, 69, 3, 4, 5, 6, 7, 9, 12, 15, 16, 14, 19, 27, 28, 34, 35, 43, 42, 44, 57, 58, 59, 61, 66, 71, 73, 1]. The dependency upon the present value of temperature is associated with increased elastic modulus for equilibrium conditions, changing viscoelastic properties, and decreased material toughness [29, 20, 11, 10, 54]. The physical mechanisms associated with these changes are usually ascribed to the statistical nature of elastomers and are thus mainly associated with conformational re-arrangement [70, 26, 23, 22, 21, 24, 25, 38, 51, 67].

The mechanical load in the present context is directly associated with the energy release rate at the crack tip. Energy release rate is the physical quantity introduced by Eshelby to characterize the driving force upon a singularity in the elastic field [17, 18] and is intimately related to the pioneering fracture studies by Ingles [36], Griffith [33], Irwin [37], and Rivlin and Thomas [56]. In the context of fracture, this driving force or energy release rate is often associated with the J-integral criteria [55, 8]; under common conditions the two are synonymous. The conversion of mechanical load to energy release rates is a complex undertaking for a spinning tire on a vehicle and is perhaps most easily approached from an approximate numerical viewpoint. There are a variety of methods available for the computation of energy release rates given mechanical loads. For the tire, one is for practical reasons restricted to methods associated with numerical approximations such as the finite element method[72]; see e.g. [49, 39] for a discussion on computational methods for energy release rates. In the computations presented below Steinmann's method [64, 65] has been employed.

3.1   Tire temperature

The determination of the thermal demands placed upon the tire materials under running conditions were performed at the BFS Texas Proving Grounds in Fort Stockton using a 1997 Ford XLT Explorer and a 1998 Ford XLT Explorer; both vehicles were four wheel drive. The 1997 Explorer was tested in

the unloaded configuration. The 1998 Explorer was tested at approximately the RGAWR (Rear gross axle weight rating) condition. The statically measured wheel loads are shown in Table 1. The vehicles were outfitted with Wilderness AT tires.

Temperature measurements were made by driving the vehicles on the test track at 105 kph and 137 kph until the thermal state of the tires stabilized. The vehicles were then stopped and needle pyrometers were used to determine the belt edge temperatures on the inside and outside shoulders. These values were then averaged to determine the wedge material temperatures. These temperature measurements are plotted in Figs. 2–5 as temperature increments over a reference temperature computed as $T_{\text{ref}} = 0.9T_{\text{ambient}} + 0.1T_{\text{pavement}}$. During the testing sequence ambient temperatures ranged from 7.8C to 35.0C and pavement temperatures ranged from 11.7C to 45C. The data is plotted versus cold inflation pressure at the ambient temperature when the vehicles were stopped; this adjustment was performed assuming the ideal gas law.

From the data one can observe:

1. At lower inflation pressures the heat build-up in the belt edge region of the rear tires is pronounced for the vehicle with a heavy cargo load.

2. Vehicle speed plays a role in heat build-up with higher speeds leading to higher belt edge temperatures.

3. Almost uniformly, the belt edge temperatures are ordered by the static loads on the tires with the largest loads leading to the hottest temperatures. For instance, at the RGAWR condition the left rear tire heats up the most and in the unloaded condition the left front tire heats up the most – though the trends do depend in a non-obvious way upon inflation pressure.

4. The magnitude of the temperature rises over the reference temperature at highway speeds and low inflation pressures can be as much as 50C at full load. On a hot day this will result in a substantial belt edge temperature.

5. The impact of tire design (AT versus ATX) upon tire temperature has not yet been established. The AT, for instance, utilizes a lower hysteresis sub-tread and a higher hysteresis tread than the ATX. The

overall rolling resistance is reported to be the same. Thus one would expect the heat build up to be similar in both models. This point, however, has not been experimentally verified.

3.2   Vehicle loads

The dynamic demands placed upon the tires by the vehicle were determined from track tests at the BFS Acuña Mexico test facility. A testing matrix was used to determine how the dynamic forces applied to the tire are affected by inflation pressure, vehicle cargo load, and vehicle speed. The primary test vehicle was a 1998 Ford XLT Explorer with 4 wheel drive. The instrumentation mainly consisted of a pair of triaxial load cells affixed to the left front and left rear tires; see Figs. 6 and 7. The load cells measure the transfer of loads from the vehicle to the tire rim. Test load cases consisted of curb weight, a cargo load equivalent to RGAWR on a Ford Ranger pickup truck, RGAWR for the Explorer, and 110% of RGAWR for the Explorer. Inflation pressures took on values of 138 kPa, 180 kPa, 207 kPa, and 242 kPa; the actual inflation pressures at test time were adjusted to match these values at 21C using the ideal gas law. Additionally, a Ford Ranger was tested at some of the same conditions as a comparison vehicle. For the purposes at hand the data permits the following observations:

1. In an Explorer with only a driver in the vehicle, the front tires experience greater loads than the rear tires. As the cargo area is loaded, the weight distribution shifts to the rear tires with the cross over point occurring around 11.6 kN on the rear axle.

2. An examination of the dynamic load histories from constant speed highway and city course driving shows that the effect of increased inflation pressure is to slightly broaden the dynamic distribution of forces on the tire; see e.g. Figs. 8 and 9 which show the histograms of the dynamic vertical loads applied by the Explorer to the left rear and left front tires on the highway course at the Ranger RGAWR condition.

3. The dynamic mean of the vertical forces on the tires is consistently below the static mean. The explanation for this phenomena has not been established but is thought not to be from load cell errors. Note that the differences between the dynamic means and the static values is less at lower speeds. An aerodynamic study of the Ford Explorer has

not been performed and is likely not warranted in the present situation given the large variance one can expect with service loads.

4. In comparing the load histories for the Ranger to that of the Explorer one can observe clear differences in the dynamic signatures. The differences, however, appear to be secondary in that they concern loading events that happen with a probability of less than 1%.

3.3   Energy release rates

Finite element analysis was performed to estimate the crack tip driving forces under normal operating conditions as determined from the road tests conducted in Acuña Mexico. Finite element analysis of a rotating tire is a computationally demanding exercise which is performed in a steady spinning frame of reference. This methodology is based upon the early work of Lynch [50] and the basic equations for such an analysis in finite deformation are presented by Oden and Lin [53]; see LeTallec and Rahier [48] or [32] for a transparent discussion of the kinematics of rolling tires in a computational setting. Steinmann's method was employed for computing the energy release rates [64, 65].

In the analysis performed, a Wilderness AT tire was modeled using dimensions measured from a cut tire section. The model was run in the simplest mode of straight-ahead free rolling with zero fore-aft loads. This permitted the use of 1/4 symmetry for increased computational efficiency. A single circumferential crack was introduced into the tire between the #1 and #2 belts starting at the #2 belt edge at depths of 1.5 mm, 10.5 mm, 25.5 mm, and 30.5 mm. The crack faces were modeled as frictionless. The model was run at inflation pressures of 138 kPa, 180 kPa, 207 kPa, and 242 kPa. Rotational velocities corresponding roughly to 60 kph and 120 kph were examined. Contact (footprint) forces up to 7.2 kN were examined. For certain conditions, the ATX tire was approximately modeled by utilizing the AT model but with the ATX end-count and belt angle. Note that steady-state rolling computations can not take into account differences in pocket design.

The reader is *cautioned* that:

1. The model that has been developed has not been proofed against experimental data. Thus, the accuracy of the results has not been established and the graphs should only be used in a comparative fashion for the determination of variable significance and understanding trends.

2. The choice of a single circumferential crack in the analysis is dictated by what is analytically and computationally possible. Physical examination of tires tells us that full circumferential cracks are not particularly common. Thus the analysis has to be appropriately interpreted. It has been shown in ideal laboratory conditions [46] that cracks between steel belts start at the belt edge, penetrate a small distance between the belts, then grow longitudinally before resuming growth between the belts. Thus it is argued that the proper interpretation of the analysis presented below is that it represents energy release rates when the crack has spread in the circumferential direction an amount where the end curvature of the crack front does not influence the central portion of the crack.

3. The model utilizes a finite deformation modified neo-Hookean model with a quadratic plus log bulk energy density for the rubber materials [31]. Incompressibility is modeled using a Q1/P0 formulation [60]. The body plys and steel belts are modeled with a finite deformation orthotropic Saint-Venant Kirchhoff model based upon the Green-Lagrange strain tensor [63]. For the body plys, the compressive stiffness in the cord direction is 2 orders of magnitude less than in extension; the switch is made based on the sign of the cord strain. The Saint-Venant Kirchhoff model can be problematic due to its energy growth properties in compression and needs to be used with care; see e.g. [13] for a discussion of appropriate growth conditions for non-linear elastic materials. In the present examples, this difficulty manifested itself in a non-physical buckling of the body ply. Results are reported below only for cases where the solutions were free of such non-physical modes.

4. Viscoelastic effects upon the energy release rates have not been considered in this study. While it is acknowledged that viscoelastic effects upon the stress state are important, their inclusion has only been made through a selection of the material moduli. Note that the fracture of natural rubber is well-known to be independent of rate and temperature over a very large range [47, 45, 29, 2]; see also [41, 52, 40] for further discussion on time dependent fracture of elastomers.

5. In the computations to follow, the crack faces are typically in compressive contact (except for very short cracks) and slide relative to each

other. It is assumed that the normal pressures are identical on opposing crack face elements directly adjacent to the crack tip. This assumption substantially simplifies the computation of the energy release rates.

6. The variables investigated below also affect the temperature state of the tire. However, for the purposes of this section, only their influence on crack tip driving forces is discussed. Their influence on crack growth resistance is discussed elsewhere.

7. In the figures to follow angular position on the tire is defined relative to the horizontal; see Fig. 10. The center of the footprint is located at $-\pi/2$ and the top of the tire is located at $\pi/2$.

An examination of the analysis results permits the following statements:

1. The energy release rates at a crack tip between the belts depends on inflation pressure below 180 kPa for cracks larger than 25.5 mm. For example, shown in Fig. 11 is the energy release rate as a function of angular position for a 25.5 mm crack; shown are four curves at the four different inflation pressures. It is clear that there is some influence of inflation pressure when it drops below 180 kPa. For the 10.5 mm and 1.5 mm cracks, pressure changes produce very small effects. It should be observed that the belt skim compound has a cut growth exponent in the neighborhood of 2.5; thus, percent variations in energy release rates result in over twofold percent changes in cut growth rates. Note that the lower inflation pressure corresponds to the lower energy release rate. Also be aware that the behavior of the curves for angular positions above 0 rad is markedly poor due to mesh coarsening in this region.

2. For the model investigated, at speeds up to 120 kph there is a modest effect of speed on the energy release rate at the tip of the crack in the center of the footprint. Figure 12, for example, compares the release rates at 60 kph and 120 kph at an inflation pressure of 180 kPa and a 4.4 kN load for a 25.5 mm crack. The observed behavior is expected to persist up to the standing wave limit.

3. In interpreting the results, note that it is actually the ΔG per revolution that matters in terms of fatigue crack growth for a natural rubber. It is, however, not clear whether one should consider the change from the

minimum to the maximum or from the value away from the footprint to the maximum. The issue revolves about the time dependent nature of crystallite freezing and melting. It is not clear whether or not the material can respond in unloading fast enough to warrant consideration of the absolute minimum when computing a ΔG for each cycle. One needs to determine whether or not the crack tip crystals persist or melt in the short time period from entering the footprint to arriving at the center of the footprint. Materials with more stable crystals would obviously have an advantage over those that have less stable crystals.

4. For a 5.3 kN load, an inflation pressure of 242 kPa, and a speed of 120 kph, crack tip energy release rate increments start out around 400 J/m^2 in the vicinity of the belt edge where there is a material stiffness discontinuity. They appear to drop slightly or remain the same to approximately 10 mm from the belt edge. Around this length the crack tip energy release rate increment begins to increase in a non-linear fashion reaching approximately 1.2 kJ/m^2 around 25.5 mm; see Fig. 13. Note the increments, i.e. the ΔG's, are computed as the difference between the peak value and the value at 0 rad.

5. The effect of load on energy release rates is shown in Fig. 14 for an inflation pressure of 242 kPa and a speed of 120 kph. The curves show a classic quadratic behavior initially. However, in the vicinity of 5 kN the effect of non-linear elasticity starts to play a role and the curves flatten out.

6. An important item of investigation is the influence of geometric parameters on energy release rates – e.g belt gauges, steel bias angles, shoulder thickness, etc. One of the primary differences between the AT and ATX models is the steel end-count and belt angle. Fig. 14 examines these variations for two different crack lengths. As can be seen, at certain loads the ATX will lead to higher crack growth rates. Using the known crack growth exponent of 2.5 for the belt skim one sees at roughly 5.25 kN that the crack growth rates in the ATX are 38% higher for a 10.5 mm crack. For the shorter crack length the crack growth rates are actually lower in the ATX design versus the AT design.

7. The release rates presented can be used to estimate the changes in lifetime for the tire based on a variety of design and usage variations. Due

to the newness of the methods used to perform the computations, these studies would presently only be valid for use in comparative analysis.

4   Tire material capacity

Tire material capacity is presented below from two different studies. The first is a survey from materials collected from returned tires. The second study is from ideal laboratory tests on virgin materials and materials subjected to accelerated aging. For the most part, neither of these studies directly measures the needed material properties to understand the tear behavior of the belt materials; however, they represent the best available information on the properties of the critical materials and are thus useful in making comparative statements. A discussion of some direct cut growth data which has been collected is presented.

4.1   Return tire survey

The return tire survey was conducted jointly by Ford and Firestone. As tires were returned to Ford dealerships as part of the recall, detailed information was gathered from the owners about tire usage; additionally tires returned to Firestone stores were collected. The tires were then labeled and cut into pieces which were distributed for material property testing to various laboratories that specialize in elastomeric compounds. The property testing focused on the wedge material and consisted of elongation to break, 100% modulus, and stress at break. Additionally, peel force experiments and a belt edge crack length survey were conducted. The reader is cautioned about one matter of significance:

1. The different laboratories have reported values showing systematic bias. In particular, the elongation to break data, the stress at break and the 100% modulus data were collected at BFS and Lab A[3]. For the three measurements mentioned, Table 2 shows from the same populations of tires the means, standard deviations, paired difference 95% confidence intervals, and the z-statistic for a null hypothesis of zero mean paired difference. With at least 95% confidence one can say that the

---

[3]The independent laboratory is identified only as Lab A in conformance with a confidentiality agreement between BFS, Ford, and the laboratory.

strain measuring methodologies at the two labs are different. Note that the stress at break is the same (within at least 95% confidence) which indicates that the load cells utilized are compatible. The 100% modulus values are of course skewed by the differing strain scales. The implication of this problem is that the absolute numbers shown below can not be relied upon. However, since the data points are intermixed computed trends and averages are still valid. Note that in the plots of elongation to break and 100% modulus that follow there are 350 tire measurements from Lab A and 463 tire measurements from BFS.

2. A more precise analysis to remove the inter-laboratory variance could be made by performing a multivariate regression with a binary predictor variable for the laboratory.

4.1.1   Tread wear

In the sections to follow, many of the material properties are plotted versus tread wear. This was used as the indicator of 'tire-time' instead of mileage or tire age as is commonly done. Tread wear for a given tire was computed by measuring the tread depth at 3 locations Serial Side (SS), Center, and Opposite Serial Side (OSS) and averaging these values. Zero percent tread wear was considered any average value above 9.8 mm. It is noted that:

1. Tread wear is not the ideal indicator of time especially when looking at fatigue processes. For fatigue analysis of strain crystallizing natural rubber the number of fatigue cycles is much more important and thus fatigue time is better correlated to tire mileage. The correlation between tread wear and mileage is approximately linear for the Wilderness AT however for the ATX tire there is no apparent correlation; see Fig. 15 for the correlation to mileage and Fig. 16 for the correlation to revolutions (fatigue cycles). The number of cycles is estimated knowing the ideal tire diameter of $235 * 1.5 + 381$ mm. For the Wilderness AT one can estimate 400,000 revolutions for each percent tread wear. For the ATX no such estimate is available.

2. It is not clear whether the mileage part of the database is accurate. Some of the listed tires have unrealistic mileages associated with them.

3. Neither tread wear nor mileage represent a good metric of time the tire has spent at an elevated temperature. It would be useful to have

such a metric to make conclusive statements concerning heat aging. Possibilities for such a metric would include items such as residual anti-oxidant, resin migration, or volatile component loss.

4.1.2   Climate designation

In the analysis to follow, the designation 'S' for southern indicates the tire was primarily used in California, Florida, Texas, Arizona, or Tennessee. Tires given the designation 'N' were primarily used in Michigan, Minnesota, Washington, or Ohio.

4.1.3   Elongation to break

From the wedge area of the returned tires small test pieces were extracted for mechanical testing to failure. As a measure of the ductility (extensibility) of the material, a standard measure is the elongational strain at break in a tension test. In the context of the present problem, this standard measure can be used as a measure of material aging; the reader is reminded that material aging refers to any evolutionary changes in crosslink and/or polymer structure. Neither a determination of the physical mechanism taking place in the material nor its cause is possible with this test.

Figure 17 shows the breaking elongation of the wedge material sorted by plant of production, tire model, and latitude of usage. The plot permits the following statements:

1. A casual visual inspection of the plot indicates that the wedge materials are aging (using elongation to break as the metric) with increasing tread wear. However a statistical analysis of the data only partially supports this observation. In particular, see Table 3 for the r^2 coefficient of determination for linear and exponential fits and the linear slope 95% confidence interval. For 7 of the 12 categories the linear slope is statistically significant; however, the coefficients of determination are somewhat small.

2. The tires utilized in the southern latitudes have a lower elongation to break than tires utilized in the north. For the ATX the mean difference between north and south to 95% confidence is 72.9±9.68 and for the AT it is 40.4±9.76. The null hypothesis z-statistics for these results are quite high; see Table 4.

3. The data supports the statement that the AT tires are superior to the ATX tires when using elongation to break as a measure of material performance; see Table 4 where these models are compared in the southern and northern categories.

4. If one examines those tires with zero tread wear then one sees similar trends; see Table 5. Presumably, heat build up from improper use would not be a large factor in the material properties of this population of tires. Yet the same trends as observed for the entire population are also observed here. Note that a zero tread wear tire does not necessarily mean that it is a new tire. It could be an unused or little used tire; e.g. it could be a spare tire.

5. One caveat to these statements is the fact that ATX tires have been in production for a longer period than AT tires. Thus age could be playing a role in some of the observed differences.

6. Firestone engineers have collected similar data on competitor tires. The numerical values reported here are fully consistent with this additional database. Though it is noted that the values associated with the Decatur plant lie at the lower end of the range of values from competitor tires.

4.1.4   100% Modulus

In conjunction with the wedge compound elongation to break tests a measurement was made of the 100% Modulus for the wedge specimens extracted from the returned tires. This measurement mainly provides an indicator of increased cure (ie. crosslink density). The assumption being made here is that the compounds under consideration are going through a polysulfidic to mono- and di-sulfidic evolution with time; this assumption is supported by lab tests shown later in the report. Under appropriate conditions this test can also provide a measure of oxidative effects such as chain scission. It can also provide an estimate of the changes in critical energy release rate which is thought to be proportional to the square-root of the molecular mass between crosslinks – a quantity that decreases with increased crosslinking [30]. Figure 18 shows the 100% modulus of the wedge material sorted by plant of production, tire model, and latitude of usage. The plot permits the following statements:

1. A casual visual inspection of the plots indicates that the wedge materials are aging (using 100% modulus as the metric) with increasing tread wear. However, a statistical analysis of the data only partially supports this observation. In particular, see Table 6 for the r^2 coefficient of determination for linear and exponential fits and the linear slope 95% confidence intervals. For 9 of the 12 categories the linear slope is statistically significant; however, the coefficients of determination are somewhat small.

2. Tires used in the warmer states are showing higher 100% modulus; see Table 7. For the ATX the mean difference from North to South is 1.93 N/mm² with a ±0.357 95% confidence interval. The z-statistic for the mean difference null hypothesis is 10.6. For the AT the mean difference is also significant, with a z-statistic of 7.8 for the standard null hypothesis, but with a value of 0.793±0.199.

3. In the warmer climates, the data supports the statement that in terms of 100% modulus AT tires possess a lower modulus versus ATX tires. Comparing AT and ATX tires in the South shows statistically significant differences. In the North, the difference between the AT and ATX means is below the 95% confidence level; the z-statistic is 1.40 and thus does not fall in the rejection regime for the standard null hypothesis of equal means.

4. If one examines those tires with zero tread wear then one sees similar trends; see Table 8. Presumably, heat build up from improper use would not be a large factor in the material properties of this population of tires. Yet the same trends as observed for the entire population are also observed here. Note that a zero tread wear tire does not necessarily mean that it is a new tire. It could be an unused or little used tire; e.g. it could be a spare tire.

5. Firestone engineers have collected similar data on competitor tires. The numerical values reported here are fully consistent with this additional database.

4.1.5 Tire Specimen Peel test

As part of the returned tire survey conducted by Firestone and Ford a number of peel test experiments were performed. This test is a direct measure of

catastrophic crack propagation. The tests utilized 1 inch wide specimens cut from the tires at 0 bias angle – i.e. parallel to the radial body ply cords. The surface tread was ground down to 4.5 mm from the top of the #2 belt. Then a razor edge was utilized to introduce a pre-crack between the belts starting at the belt edge. The test pieces were loaded into a tension testing machine and pulled apart. The primary quantity of interest in this experiment is the average force during tearing as it can be directly related to the critical energy release rate for the inter-belt crack.

Experimental Data   Shown in Fig. 19 are the peel forces in Newtons over a reference 25.4 mm section width. The data is separated by production plant, tire model, and latitude of usage.
   The plot allows one to draw several inferences.

1. There is no evidence of correlation between the variance in tread wear and that of peel force. See Table 9 which shows the r^2 coefficient of determination values for linear and exponential fits and the linear slope 95% confidence interval. The linear slope is statistically significant for only 1 of the 12 categories.

2. Looking at Tables 10 and 11 one notes that AT's in the north are slightly better than AT's in the south. A similar statement about the ATX is not possible due to statistical variance.

3. Southern AT's are performing above Southern ATX's though the spread is somewhat large. No such statement can be made concerning Northern AT's and ATX's.

4. The Decatur population of tires is providing a statistically significant lower peel force versus that seen in Wilson or Joliette tires. This holds for both the Northern and Southern tire populations. The trend is also present in the population of tires with zero tread wear – though the variance is somewhat larger.

5. A closer examination of four of the peel test specimens reveals some evidence for the differences between the data points. In particular, if one examines the morphology of the torn failure surfaces then one sees a different crack tip phenomena. Shown in Figs. 20 and 21 are photographs of the torn surfaces from a tire manufactured in Decatur

and Wilson, respectively. Tire F44 was manufactured in the 49th week of 1997 and used for 23,000 miles in Florida; F89 was manufactured in the 33rd week of 1997 and used for 31,000 miles in Texas. The tear force on the peel test for F44 was 56 N and for F89 was 76 N. These photographs suggest that the higher strength F89 tire is showing a 'knotty tear' whereas the F44 tire displays a much smoother failure surface indicating a suppression of crystallite formation at the crack tip. Such a transition in fracture mechanism could easily account for the difference in peel forces. A closer view of such morphological differences is shown in Figs. 22 – 25 which are 11X and 12X scans from an electron microscope for a Decatur and a Wilson tire peel test. Tire F33 was manufactured in the 14th week of 1998 at Decatur and used for 35,000 miles in Arizona; F199 was manufactured in the 5th week of 1998 at Wilson and used for 15,000 miles in Texas. The tear force on the peel test for F33 was 55 N and for F199 was 97 N. The micrographs show clear differences.

6. An examination of the force versus displacement graphs for 20 additional peel tests also supports the previous observations. In particular, the graphs show very smooth curves for the samples from Decatur and noticeably rougher curves for the samples from Wilson. There is some experimental evidence in the literature [47] to suggest that these observations are compatible with the hypothesis of reduced crack tip crystallization in the Decatur samples. (Note, for strain crystallizing natural rubber rate and temperature effects are rather modest.)

7. Some very limited belt to belt peel tests conducted using new tires manufactured in Wilson and Decatur in February and May 2000 also support these observations. This data shows Wilson tires have a peel force nearly double that of Decatur tires – 183 N / 25.5 mm versus 103 N / 25.4 mm. Similar peel tests were also performed by assembling belt packages in the laboratory using components manufactured in the different plants during October 2000. These peel tests showed similar plant differences – 137 N / 25.4 mm versus 89 N / 25.4 mm.

Estimation of Critical Energy Release Rates   The peel forces are directly related to the critical energy release rate required to propagate a crack between the belts. The classical analysis of experiments of this type is ap-

parently due to Rivlin and Thomas [56]. If one ignores the extensibility of the peel legs then the critical energy release rate is simply given as

$$G_c = 2P/w \,, \tag{1}$$

where w is the width of the test piece and P is the peel force. The inclusion of the extensibility gives

$$G_c = (\lambda_1 + \lambda_2)P/w - (W_1 t_1 + W_2 t_2) \,, \tag{2}$$

where λ_1 and λ_2 are the stretches of the two legs of the test specimen, W_1 and W_2 are the strain energies of the legs, and t_1 and t_2 are the thicknesses of the legs. If the force extension ratio for each leg is given linearly as $P_i = C_i(\lambda_i - 1)$ then Eq. (2) takes on its well known quadratic form:

$$G_c = \frac{P}{w} \left[P \frac{C_1 + C_2}{2C_1 C_2} + 2 \right] \,. \tag{3}$$

These formulae are rather robust even though they do not account for all the non-linear features of the test set up. To assess the simplified formulae a finite element simulation was conducted for an idealized peel test specimen. Shown in Fig. 26 is the finite element mesh at high extension. From such a simulation, one can extract the energy release rate at the crack tip by averaging the singular part of Eshelby's energy-momentum tractions across the width of the specimen [64, 65]. Figure 27 shows the results of such a simulation using the geometric and material properties from the AT and ATX tires. Also shown in the figure is Eq. (3) using estimates for the C_i's. From the figure one can note:

1. The simplified formula is modestly accurate over the range of interest in the experiments.

2. There is a slight amount of non-linearity in the material response of the test piece which makes Eq. (3) under-predict below 50 N and over-predict above 50 N.

3. The non-linearity of the release rate versus peel force also shows that the higher peel force values do not indicate as high of a critical energy release rate value as one might expect based on simplified analysis. This is important since it slightly reduces the differences between the plants when the peel force values are converted to the proper governing material property. Shown in Table 12 are the mean values from the peel force experiments converted into critical energy release rates.

4.1.6   Belt edge crack survey

For a small population of the returned tires, (482 tires), a survey was made for the presence of belt edge cracks. To make these determinations, the tires were sliced in two along a diameter. Then from the exposed surfaces 4 measurements were made of the belt edge crack lengths and these were averaged for plotting purposes. Data points for tires that did not show any belt edge cracks along this cut were not plotted. Shown in Fig. 28 is a plot of this data versus tread wear with the data sorted by production plant, tire model, and latitude of usage. The sampling methodology of the population makes it difficult to make definitive statements that sort one population from another; it would have been better to have made a complete 360° survey of the tires for cracks. One can, however, still state:

1. The rate of crack detection using the given methodology in tires from the southern latitudes was 3 times higher than that for the northern latitudes at Wilson and Joliette, and 5 times higher at Decatur; see Table 13 which shows the belt edge separation detection rates and total sample sizes. The actual significance of these comparisons and their absolute values is not straightforward given the sampling methodology utilized. In particular, it is noted that simply examining the tire at two locations circumferentially could easily miss cracks in the belt edge region. The table is provided for completeness but should be used with caution.

2. If one assumes the examination points are independent events (which they are not exactly) then one can easily estimate the amount of circumferentially cracked belt edge for the different populations. Doing so indicates that for Wilson and Joliette South there is roughly 65° of cracked belt edge where as for Decatur South there is only roughly 26°. For Wilson and Joliette North there is roughly 20° of cracked belt edge where as for Decatur North there is only roughly 4°. Better estimates can be made from this data by accounting for the spatial correlation between sampling points, however, the trend will still be the same. Casually, one would expect that the detection rate would be higher for the population of "weaker tires". The present data, then, runs counter to elongation to break, 100% modulus, and peel force data from the returned tires.

3. Given that crack length should be related to the number of revolutions of the tire it makes sense to plot the data versus mileage. However, for the tires shown in Fig. 28, mileage is only known for 75 tires. Due to this low number, a plot of belt edge separation versus mileage provides no real usable information. With additional data points such a plot could be used to obtain *in situ* cut growth curves. For completeness the plot of BES versus mileage is shown in Fig. 29. The values are seen to be consistent with the estimated release rates from the finite element analysis and the cut growth data presented later in the report.

4.2 Standard lab tests to probe the effect of lubricant influence

The return survey data shows that there are differences in the performance levels of the same nominal materials[4] at different production plants. In particular, for tires manufactured at Decatur the peel forces are significantly lower. This leads one to investigate the exact differences in the material processing methods at these facilities. The primary difference that can be observed is in the early mixing stages. At Decatur the materials are mixed in a Banbury and then extruded, chopped into small pellets, and then coated by lubricants so that they do not stick together. At the plants in Wilson and Joliette the materials are also mixed in a Banbury but then they are calendared into wide sheets followed by a lubricant coating. It is also noted that the lubricants used in the facilities are not the same. The base lubricant is a metal oxide but in Decatur it is augmented by the addition of a detergent. Thus at Decatur, the materials are exposed to a different lubricant and further, since the form factor of the material is different during the lubrication stage, the material in Decatur possesses a higher weight percentage of lubricant entrained in the rubber stocks. For the stocks in question, one can estimate from single pass factory quality control data that the Decatur stock will have a range of 0.8% to 2.4% lubricant weight pickup and Wilson stocks a range of 0.08% to 0.21% [5]. Since lubricants are low molecular weight components that are free to migrate, cause chain scission, and/or interfere

---

[4]The assumption here is that J2757 and J2917 are manufactured from the same exact set of ingredients at all plants.

[5]Firestone engineers have indicated that final pass data shows that Decatur stocks have a range of 1.5% to 2.5% and that Wilson stocks have a maximum pickup of 0.5%.

with chemical reactions it is important to investigate their influence on the material properties.

The pick-up of the lubricant is an order of magnitude lower using the system in place at Wilson and Joliette. This point needs to be kept in mind when comparing materials in the sections to follow, where for testing purposes batches of J2757 and J2917 were mixed with differing amounts and types of lubricant. In what follows, these different batches are simply referred to as Decatur J2757, Wilson J2757, etc., where the plant designation is employed to distinguish between lubricant formulae and not to indicate that the materials were actually collect at the plants. The tests shown below were conducted by BFS and represent a portion of the BFS standard battery of tests.

4.2.1   Ring tests

The ring tensile test is a standard BFS laboratory test for comparing materials. In this test a ring of material is stretched to breaking in a tension testing machine. From these tests, data on 100% extensional modulus and ring toughness[6] have been extracted for all batches. This data is shown in Figs. 30-31 plotted versus percent lubricant for aged and un-aged materials. The aging was performed in an O_2 environment at 100C for 2 days; all samples were tested at room temperature.

If one compares the properties of the two materials at their actual lubricant weight percentage ranges for the two plants, then one can note:

1. There is a strong temptation to draw inferences about the effect of lubricant for the 100% modulus by looking at the plots. However, for most cases there is not enough statistical evidence to draw conclusions; see Table 14. In particular, the correlation with 100% modulus and lubricant percentage is only justified for unaged J2917.

2. For the ring toughness one is not justified from the collected data in drawing any conclusions with regard to lubricant content and ring toughness for either material; see Table 15.

---

[6]Ring toughness is the product of the percent elongation at break multiplied by the ring (engineering) stress at break.

4.2.2   Laboratory peel test

The one-inch adhesion test is a laboratory test that is directly related to catastrophic tearing. In this test a one inch wide specimen is formed by curing together two layers of rubber whose adhesion one wishes to examine. The layers of rubber are backed by stiff materials to reduce the extensibility of the peel test legs; see Fig. 32. Further a very stiff nylon mesh is placed between the two layers of the rubber to force the peel to occur at the interface between the layers; the rubber does not adhere to the nylon fabric in any appreciable way. The entire assembly is press cured together before testing in a tensile testing machine.

The critical energy release rate for the adhered materials can in principle be extracted from this experiment. The difficultly in doing so arises from the presence of the mesh which induces a complex geometry upon the failure front in the test setup. The front is actually similar to an array of small square tension test specimens; see Fig. 33. This makes the connection between specimen leg extension and new cracked area non-trivial. Thus the test can only be utilized for comparative analysis.

Shown in Fig. 34 are the peel forces for the material batches versus lubricant weight percentages. The top of the figure shows the results for J2917 and the bottom of the figure the results for J2757. Keeping in mind the actual ranges at each plant for the lubricant pick-up, one can note:

1. For J2917, the Decatur lubricant level versus Wilson lubricant level shows an approximately 20% lower critical energy release rate in the un-aged state. The r^2 coefficient of determination and the 95% confidence intervals indicate that the trend is statistically significant. However, there insufficient data to draw inferences about the effect of lubricant upon the peel strength in aged J2917.

2. For J2757, the material using Decatur lubricant versus that using Wilson lubricant shows an approximately 25% lower critical energy release rate; this is for aged and un-aged material. However, the 95% confidence intervals are sufficiently large that one can not conclude that this observation is statistically significant.

3. Some very limited tests were also performed using stocks made in the plants in October 2000. With these tests the plant differences are still present at 254 N / 25.4 mm versus 214 N / 25.4 mm. Note that this

test appears not to be as sensitive to plant variations as the tire sample peel tests or the laboratory belt package peel tests.

4.2.3   Cut growth study

Given the visually based hypothesis of a propagating fatigue crack between the belts, the cut growth behavior of the wedge compound and the belt skims needs to be measured in order to give an estimate of the fatigue life of the tires. Cut growth experiments under repeated loads using pure shear sheets were employed to obtain cut growth rates for both compounds (J2917 and J2757 at 0%, 1%, and 2.5% lubricant weight percentages). To date this data has been obtained for only two energy release rates with no oven aging – providing only two data points for each material batch. However, for J2757 cut growth data has been obtain for 0% lubricant over 1.5 decades of energy release rates for unaged and surface protected 6 and 12 day aged samples. The aging was performed at 80C.

From this data, shown in Fig. 35, one can observe the following points:

1. The critical release rates for J2757 are in the vicinity of 10 kJ/m^2.

2. The 6 and 12 day aged samples show changes in cut growth rates in the 1 to 10 kJ/m^2 range. Below 1 kJ/m^2 the effect of aging has not been established. Note that the tire is estimated to primarily operate in the neighborhood of 0.4 kJ/m^2.

3. Shown in Fig. 35 are two fits to Paris' law,

$$\frac{dc}{dN} = A \Delta G^n \,. \tag{4}$$

   The exponent for the aged material is roughly $n = 2.5$ and the pre-factor is roughly $A = 8.2\text{e-}8$ nm/(J/m^2)$^{2.5}$. The un-aged material has an exponent of roughly $n = 1.5$ and the pre-factor is roughly $A = 8.2\text{e-}5$ nm/(J/m^2)$^{1.5}$. These fits are valid above 1 kJ/m^2.

4. This data can be put together with the energy release rate computations from earlier in the report to give a picture of how crack evolution takes place in such tires. In terms of load, one estimates that for each 1 kN increment of tire load (in the 4 kN to 7 kN range) there will be a 50% increase in crack growth rates for the shorter crack lengths. When

the cracks approach 30 mm in depth the release rates for expected tire loads start to move into the 1+ kJ/m^2 range. At this stage the crack growth rates start to become substantial and one can expect rapid loss of structural integrity. Note that the peel force data shows critical values in the neighborhood of 5 kJ/m^2.

5   Conclusions

This study has found no single causative agent for the tire failures. It has found a number of comparative differences in tire models that are likely related to the tire failures and these are summarized below. The primary issue that impedes additional progress is the lack of established criteria for different types of tire failures. Development of such criteria is only today becoming scientifically and technologically possible.

5.1   The effect of climate and production plant

There is a correlation between actual tires used in warmer climates and three indicators of degraded material properties in the belt region of the tire. Further there is a correlation between the Decatur manufacturing plant and degraded critical energy release rates (critical crack tip driving forces) for the belt skim stocks.

1. Decreases in wedge stock ductility for both the ATX and AT shows a correlation with warmer climates.

2. Ductility of the wedge stocks for the ATX tires are lower compared to the AT tires; note age could be a factor on this point as the AT model is a newer model than the ATX.

3. 100% modulus of the wedge stocks shows a dependence upon climate. Tires in warmer climates display higher modulus values indicating an increasing level of cure. The difference between ATX tires in the north and south is nearly double that for AT tires. Similar to the ductility results there are clear differences between the AT and ATX populations but this observation may not be causative due to the age issue.

4. Peel force tests from returned tires show that tires from warmer climates possess marginally lower critical tear energies.

5. Peel force tests also show that tires from the Decatur plant have critical tear energies which are inferior to those found in tires manufactured in Wilson or Joliette when comparing similar models from similar climates. This difference is supported by a change in crack tip mechanism between plants.

6. The trends for elongation to break, 100% modulus, and peel force hold up for tires that are showing zero percent tread wear. Thus it appears that climate effects are outweighing usage effects relative to these three measures. In fact peel tests from new tires and from laboratory prepared belt packages with new materials from the different plants also support these observations.

5.2   Plant processing differences

The primary producers of the AT and ATX tires were the plants in Decatur, Wilson, and Joliette. The statistical distribution of warranty claims shows that the tires produced in the Decatur plant were implicated a disproportionate number of times. The peel force data also indicates that a critical material property is inferior in tires produced in Decatur in comparison to those manufactured in Wilson and Joliette. It has been conjectured that the differences in material processing could be contributing to these observations. A tour of the material processing facilities at the plants shows that the primary difference between the plants involves the early material mixing stages which results in the production of materials with differing weight percentages of processing lubricant. While the conjecture has not yet been refuted, to date there is insufficient data to substantiate it either.

1. As is well known, aging of belt materials substantially alters their ring toughness and 100% modulus. The hypothesis that lubricant type and levels at Decatur are contributing to the degradation of material properties could not be established from the available experimental data.

2. A BFS one inch standard laboratory peel test shows that the critical energy release rates for J2917 in the un-aged state with Decatur lubricant are dependent (negatively) upon lubricant levels. This correlation could not be shown present in the aged stocks in a statistically significant manner. In this test J2757 shows possible lubricant sensitivity to

Decatur lubricant for both aged and un-aged stocks. There is insufficient evidence to refute the statement that J2757 shows no sensitivity to Wilson lubricant.

3. The effect of lubricant upon cut growth rates and fatigue crack propagation has not yet been fully established, nor has the effect of aging been fully established with respect to fatigue cracking. Preliminary data suggests that aging plays a role in the $1+ \text{ kJ/m}^2$ release rate range but not at lower release energy rates where most of the crack growth time takes place. The effect of lubricant has not been established for this data.

5.3 Thermal demands

The climate related degradation of properties that was seen in the return tire survey points to the importance temperature plays in material behavior. Likewise, aging studies on ideal laboratory specimens show a measurable effect of thermal and oxidative aging. There are two major contributors to the temperature of the tire: (1) is the ambient temperature and (2) is the heat generation from within the tire.

1. Low inflation pressure, highway speeds, and heavy cargo loads all play a negative role in terms of contributing to thermal aging. When all three factors are present, the temperature rise in the belt region of the tire can be as high as 50C over the ambient temperature.

2. When carrying heavy loads and at high speeds, decreased inflation pressure can substantially increase tire temperature.

5.4 Energy release rate demands

The computed energy release rate demands provide a point of reference to understand how fast cracks will actually grow in these tires. Actual lifetime predictions are not made due to the enumerated caveats associated with these computations and material data need to effect the predictions. Simply put, quantitative lifetime predictions are not within the reach of present day technology. An improvement of this situation is feasible but would require a large effort by a broad team of experts. The computations do, however, provide a basis from which one can estimate the importance of various factors

on tire lifetime. It is seen from these estimates that vehicle load plays a dominant role.

1. Vehicle loads play a more important role than inflation pressure and speed in energy release rate demands. In fact, for cracks below 10.5 mm inflation pressure plays almost no role in energy release rate values. Likewise, the difference between city and highway speeds provides only small increases in energy release rates for cracks below 10.5 mm.

2. The effect of lower inflation pressures on dynamic loads is to narrow their dynamic distribution. The mean of the dynamic load is not substantially affected by inflation pressure.

3. Changes in energy release rates can have a large influence on crack growth rates due to the magnitude of the fatigue growth exponent. For example, 10% increases in energy release rates can lead to 27% increases in crack growth rates for the belt skims. The absolute rate that would be acceptable for any given tire is an unknown quantity.

4. The ATX design produces higher crack growth rates for cracks of certain lengths and particular loads. Given the crack growth exponent of the belt skims, some of these differences are substantial. In other regimes, notably very short crack lengths, the rates of crack growth are smaller in the ATX design.

Acknowledgements

References

[1] (anonymous), *Remarks on the changes of gutta percha under tropical influences*, Journal of the Chemical Society **13** (1861), 87–90.

[2] M.A. Ansarifar and G.J. Lake, *On the mechanics of rubber-to-metal bond failure*, Journal of Adhesion **53** (1995), 183–199.

[3] M. Ballauff and B. A. Wolf, *Degradation of chain molecules: 1. Exact solution of the kinetic equations*, Macromolecules **14** (1981), 654–658.

[4] R. M. Barber, *Nature of the diffusion process in rubber*, Nature **140** (1937), 106.

[5] J. P. Berry and W. F. Watson, *Stress relaxation of peroxide and sulfur vulcanizates of natural rubber*, Journal of Polymer Science **18** (1955), 201–213.

[6] E. M. Bevilacqua, *The reaction of molecular oxygen with rubber*, Rubber Chemistry and Technology **30** (1956), 667–680.

[7] F. A. Bovey and F. H. Winslow, *Macromolecules: An introduction to polymer science*, Academic Press, 1979.

[8] B. Budiansky and Rice. J.R., *Conservation laws and energy-release rates*, Journal of Applied Mechanics **40** (1973), 201–203.

[9] F. Bueche, *Mechanical degradation of high polymers*, Journal of Applied Polymer Science **4** (1960), 101–106.

[10] P. Chadwick, *Thermo-mechanics of rubberlike materials*, Philosophical Transactions of the Royal Society of London **276A** (1974), 371–403.

[11] P. Chadwick and C.F.M. Creasy, *Modified entropic elasticity of rubber-like materials*, Journal of the Mechanics and Physics of Solids **32** (1984), 337–357.

[12] K. K. Chee, *Kinetic study of random chain scission by viscometry*, Journal of Applied Polymer Science **41** (1990), 985–994.

[13] P.G. Ciarlet, *Mathematical elasticity, volume 1: Three dimensional elasticity*, North-Holland, Amsterdam, 1988.

[14] K. L. DeVries, R. H. Smith, and B. M. Fanconi, *Free radicals and new end groups resulting from chain scission:1. y-irradiation of polyethylene*, Polymer **21** (1980), 949–956.

[15] R. Ding, A. I. Leonov, and A. Y. Coran, *A study of the vulcanization kinetics of an accelerated-sulfur sbr compound*, Rubber Chemistry and Technology **69** (1996), 81–91.

[16] H. S. Dweik and G. Scott, *Mechanisms of antioxidant action: Aromatic nitroxyl radicals and their derived hydroxylamines as antifatigue agents for natural rubber*, Rubber Chemistry and Technology **57** (1984), 735–743.

[17] J.D. Eshelby, *The continuum theory of lattice defects*, Solid State Physics, Advances in Research and Applications (F. Seitz and D. Turnbull, eds.), vol. III, Academic Press, 1956, pp. 79–119.

[18] _____, *The elastic energy-momentum tensor*, Journal of Elasticity **5** (1975), 321–335.

[19] B. M. Fanconi, K. L. DeVries, and R. H. Smith, *Free radicals and new end groups resulting from chain scission:2 mechanical degradation of polyethylene*, Polymer **23** (1982), 1027–1033.

[20] J. D. Ferry, *Viscoelastic properties of polymers*, John Wiley & Sons, 1961.

[21] P. J. Flory, *Thermodynamics of high polymer solutions*, The Journal of Chemical Physics **10** (1942), 51–61.

[22] _____, *Principles of polymer chemistry*, Cornell University Press, 1953.

[23] _____, *Statistical mechanics of chain molecules*, John Wiley & Sons, 1969.

[24] _____, *Statistical thermodynamics of random networks*, Proc.R.Soc.Lond. **351** (1976), 351–380.

[25] _____, *Molecular theory of rubber elasticity*, Polymer **20** (1979), 1317–1320.

[26] P. J. Flory and J. Rehner, *Statistical mechanics of cross-linked polymer networks*, The Journal of Chemical Physics **11** (1943), 512–520.

[27] P. Fordyce, K. L. DeVries, and B. M. Fanconi, *Chain scission and mechanical degradation of polystyrene*, Polymer Engineering and Science **24** (1984), 421–427.

[28] L. H. Gan, S. C. Ng, and K. K. Chee, *Kinetic study of oxidative scission in natural rubber by wallace plasticity measurements*, Rubber Chemistry and Technology **65** (1992), 1–6.

[29] A.N. Gent, *Strength of elastomers*, Science and Technology of Rubber, 2nd Edition (J.E. Mark, B. Erman, and F.R. Eirich, eds.), Academic Press, 1994, pp. 471–512.

[30] A.N. Gent, S.-M. Lai, C. Nah, and C. Wang, *Viscoelastic effects in cutting of tearing of rubber*, Rubber Chemistry and Technology **67** (1994), 610–618.

[31] S. Govindjee and P.A. Mihalic, *Computational methods for inverse deformations in quasi-incompressible finite elasticity*, International Journal for Numerical Methods in Engineering **43** (1998), 821–838.

[32] ———, *Viscoelastic constitutive relations for the steady spinning of a cylinder*, Tech. Report UCB/SEMM-98/02, University of California Berkeley, Department of Civil Engineering, 1998.

[33] A.A. Griffith, *The phenomena of rupture and flow in solids*, Philosophical Transactions of the Royal Society of London **221A** (1920), 163–197.

[34] S. H. Hamid, M. B. Amin, and A. G. Maadhah, *Handbook of polymer degradation*, Marcel Dekker Inc., 1992.

[35] A. Inaba and T. Kashiwagi, *A calculation of thermal degradation initiated by random scission. 1 steady-state radical concentration*, Macromolecules **19** (1996), 2412–2419.

[36] C.E. Ingles, *Stresses in a plate due to the presence of cracks and sharp corners*, Transactions of the Institute of Naval Architects **55** (1913), 219–241.

[37] G.R. Irwin, *Fracture dynamics*, pp. 147–166, American Society for Metals, 1948.

[38] H. M. James and E. Guth, *Theory of the elastic properties of rubber*, The Journal of Chemical Physics **11** (1943), 455–488.

[39] K. Kishimoto, S. Aoki, and M. Sakata, *Dynamic stress intensity factors using ĵ-integral and finite element method*, Engineering Fracture Mechanics **13** (1980), 387–394.

[40] W.G. Knauss, *On the steady propagation of a crack in a viscoelastic sheet: Experiments and analysis*, Deformation and Fracture of High Polymers (Kausch, Hassell, and Jaffee, eds.), Plenum Press, 1974, pp. 501–541.

[41] W.G. Knauss and H. Dletmann, *Crack propagation under variable load histories in linearly viscoelastic solids*, International Journal of Engineering Science **8** (1970), 643–656.

[42] A. M. Kotliar, *Correlation of the change of the intrinsic viscosity with random chain scission*, Joural of Polymer Science **51** (1961), S64–S64.

[43] A. M. Kotliar and A. D. Anderson, *The influence of the initial molecular weight distribution on the molecular weight averages for polymers undergoing crosslinking and chain scission*, Journal of Polymer Science **45** (1960), 541–546.

[44] M. R. Krejsa and J. L. Koenig, *A review of sulfur crosslinking fundamentals for accelerated and unaccelerated vulcanization*, Rubber Chemistry and Technology **66** (1993), 376–409.

[45] G.J. Lake, *Fatigue and fracture of elastomers*, Rubber Chemistry and Technology **68** (1995), 435–460.

[46] _____, *Application of fracture mechanics to crack growth in rubber-cord laminates*, (2000), In submission.

[47] G.J. Lake, A. Smasuri, S.C. Teo, and J. Vaja, *Time-dependent fracture in vulcanized elastomers*, Polymer **32** (1991), 2963–2975.

[48] P. Le Tallec and C. Rahier, *Numerical models of steady rolling for nonlinear viscoelastic structures in finite deformations*, International Journal for Numerical Methods in Engineering **37** (1994), 1159–1186.

[49] F.Z. Li, C.F. Shih, and A. Needleman, *A comparison of methods for calculating energy release rates*, Engineering Fracture Mechanics **21** (1985), 405–421.

[50] F. DE S. Lynch, *A finite element method of viscoelastic stress analysis with application to rolling contract problems*, International Journal for Numerical Methods in Engineering **1** (1969), 379–394.

[51] J. E. Mark and B. Erman, *Rubberlike elasticity: A molecular primer*, John Wiley & Sons, 1988.

[52] H.K. Müller and W.G. Knauss, *Crack propagation in a linearly viscoelastic strip*, Journal of Applied Mechanics **38E** (1971), 483–488.

[53] J.T. Oden and T.L. Lin, *On the general rolling contact problem for finite deformations of a viscoelastic cylinder*, Computer Methods in Applied Mechanics and Engineering **57** (1986), 297–367.

[54] S. Reese and S. Govindjee, *Theoretical and numerical aspects in the thermo-viscoelastic material behaviour of rubber-like polymers*, Mechanics of Time-Dependent Materials **1** (1998), 357–396.

[55] J.R. Rice, *A path independent integral and the approximate analysis of strain concentration by notches and cracks*, Journal of Applied Mechanics **35** (1968), 379–386.

[56] R.S. Rivlin and A.G. Thomas, *Rupture of rubber 1. Characteristic energy for tearing*, Journal of Polymer Science **10** (1953), 291–318.

[57] R. M. Russell, *Changes in the chemical structure of natural rubber tyre vulcanisates in service*, Br.Polym. J. **1** (1969), 53–58.

[58] M. S. Sambhi, *Kinetics of chain scission of natural rubber*, Rubber Chemistry and Technology **62** (1989), 779–787.

[59] R. Simha, *Kinetics of degradation and size distribution of long chain polymers*, Journal of Applied Physics **12** (1941), 569–578.

[60] J.C. Simo and R.L. Taylor, *Quasi-incompressible finite elasticity in principal stretches. Continuum basis and numerical algorithms*, Computer Methods in Applied Mechanics and Engineering **85** (1991), 273–310.

[61] T. D. Skinner, *The cbs-accelerated sufuration of natural rubber and cis-1,4-polybutadienne*, Rubber Chemistry and Technology **45** (1972), 182–192.

[62] S.B. Smeulders and S. Govindjee, *A phenomenological model of an elastomer with an evolving molecular weight distribution*, Journal of Rheology **43** (1999), 393–414.

[63] A.J.M Spencer, *Constitutive theory for strongly anisotropic solids*, Continuum Theory of the Mechanics of Fibre-Reinforced Composites (A.J.M Spencer, ed.), Springer-Verlag, Wien, 1984, pp. 1–32.

[64] P. Steinmann, *Application of material forces to hyperelastic fracture mechanics. I. Continuum mechanical setting*, International Journal of Solids and Structures **37** (2000), 7371–7391.

[65] P. Steinmann, D. Ackermann, and F.J. Barth, *Application of material forces to hyperelastic fracture mechanics. II. Computational setting*, International Journal of Solids and Structures (2001), (to appear).

[66] M. Tirrell and M. F. Malone, *Stress-induced diffusion of macromolecules*, Journal of Polymer Science, Polymer Physics Edition **15** (1977), 1569–1583.

[67] L. R. G. Treloar, *The physics of rubber elasticiy*, Oxford University Press, 1958.

[68] G. J. van Amerongen, *Influence of carbon black on the oxidation of natural rubber*, Industrial Engineering Chemistry **45** (1953), 377–379.

[69] _____, *Oxidative and nonoxidative thermal degradation of rubber*, Industrial Engineering Chemistry **47** (1955), 2565–2574.

[70] J. H. Weiner, *Statistical mechanics of elasticity*, John Wiley and Sons, 1983.

[71] J. Zhou, *A constitutive model of polymer materials including chemical ageing and mechanical damage and its experimental verification*, Polymer **34** (1993), 4252–4256.

[72] O.C. Zienkiewicz and R.L. Taylor, *The finite element method, volume 1*, 5 ed., Butterworth and Heinemann, 2000.

[73] R. M. Ziff and E. D. McGrady, *Kinetics of polymer degradation*, Macro-molecules **19** (1986), 2513–2519.

A   Tables

Table 1: Static vertical loads (kN) on tires for temperature tests.

	Unloaded Vehicle		Loaded Vehicle	
	Left	Right	Left	Right
Front	6.0	4.9	5.7	5.1
Rear	4.6	4.7	6.7	6.3

Table 2: Laboratory differences for 167 tires that were tested at both BFS and Lab A.

Measurement	Lab	Mean	Std. Deviation	Paired Difference 95% CI	$z(H_o : \mu_D = 0)$
% Elongation to break	Lab A	240.4	50.0	13.37±4.18	6.27
	BFS	227.1	51.9		
Stress at break (N/mm^2)	Lab A	16.0	2.06	0.0574±0.218	0.517
	BFS	15.9	2.52		
100% Modulus (N/mm^2)	Lab A	5.71	1.25	0.573±0.113	9.96
	BFS	6.29	1.19		

Table 3: r^2 regression values for elongation to break versus tread wear, 95% confidence intervals for slope of linear fit.

Category	r^2 linear-fit	Slope 95% CI	r^2 exponential-fit
Decatur N ATX	0.2123	-0.827±0.605	0.1743
Decatur N AT	0.3823	-1.20±0.432	0.4051
Wilson N ATX	0.1349	-0.512±0.546	0.1401
Wilson N AT	0.3889	-1.92±0.633	0.4248
Joliette N ATX	0.3693	-0.750±0.445	0.3622
Joliette N AT	0.0033	0.0556±0.345	0.0019
Decatur S ATX	0.5045	-0.866±0.232	0.4929
Decatur S AT	0.5906	-1.09±0.238	0.5869
Wilson S ATX	1.37e-7	0.001±0.576	0.0008
Wilson S AT	0.4365	-2.14±0.592	0.4540
Joliette S ATX	0.3819	-1.15±0.526	0.3651
Joliette S AT	0.0530	-0.440±0.558	0.0405

Table 4: Means and standard deviations for elongation to break by latitude and tire model. 95% confidence intervals for population comparisons with z-statistic.

Category	Mean	Std. Deviation	Mean Difference 95% CI	z-statistic
Southern ATX	175.5	33.8	72.9±9.68	14.8
Northern ATX	248.4	34.3		
Southern AT	234.3	43.1	40.4±9.76	8.11
Northern AT	274.7	45.6		
Southern ATX vs Southern AT			58.8±8.83	13.0
Northern ATX vs Northern AT			26.3±10.5	4.88

Table 5: Means and standard deviations for elongation to break by latitude and tire model at zero percent tread wear. 95% confidence intervals for population comparisons with z-statistic.

Category	Mean	Std. Deviation	Mean Difference 95% CI	z-statistic
Southern ATX	185.7	28.9	87.0±17.4	10.0[a]
Northern ATX	272.8	30.8		
Southern AT	261.1	34.8	39.6±16.0	4.84
Northern AT	300.6	44.8		
Southern ATX vs Southern AT			75.3±17.8	8.46[b]
Northern ATX vs Northern AT			27.9±18.7	2.96[c]

[a]t-statistic is used here; $t_{0.025} = 2.012$
[b]t-statistic is used here; $t_{0.025} = 2.001$
[c]t-statistic is used here, $t_{0.025} = 1.989$

Table 6: r^2 regression values for 100% modulus versus tread wear.

Category	r^2 linear-fit	Slope 95% CI	r^2 exponential-fit
Decatur N ATX	0.1279	0.016±0.016	0.1743
Decatur N AT	0.1075	0.018±0.014	0.4051
Wilson N ATX	0.1663	0.015±0.014	0.1401
Wilson N AT	0.1058	0.012±0.009	0.4248
Joliette N ATX	0.3358	0.018±0.012	0.3622
Joliette N AT	0.1179	-0.010±0.010	0.0019
Decatur S ATX	0.1243	0.027±0.020	0.4929
Decatur S AT	0.2609	0.019±0.008	0.5869
Wilson S ATX	0.0258	0.008±0.020	8.3e-4
Wilson S AT	0.3626	0.031±0.010	0.4540
Joliette S ATX	0.1676	0.035±0.028	0.3615
Joliette S AT	0.1032	-0.017±0.015	0.0405

Table 7: Means and standard deviations for 100% modulus by latitude and tire model. 95% confidence intervals for population comparisons with z-statistic.

Category	Mean (N/mm^2)	Std. Deviation	Mean Difference 95% CI	z-statistic
Southern ATX	7.31	1.68	1.93±0.357	10.6
Northern ATX	5.39	0.86		
Southern AT	6.01	0.96	0.793±0.199	7.80
Northern AT	5.22	0.87		
Southern ATX vs Southern AT			1.30±0.335	7.62
Northern ATX vs Northern AT			0.168±0.235	1.40

Table 8: Means and standard deviations for 100% modulus by latitude and tire model at zero percent tread wear. 95% confidence intervals for population comparisons with z-statistic.

Category	Mean (N/mm^2)	Std. Deviation	Mean Difference 95% CI	z-statistic
Southern ATX	6.75	1.13	1.94±0.517	7.56[a]
Northern ATX	4.81	0.66		
Southern AT	5.39	0.86	0.301±0.326	1.81
Northern AT	5.09	0.70		
Southern ATX vs Southern AT			1.36±0.522	5.22[b]
Northern ATX vs Northern AT			0.283±0.315	1.78[c]

[a]t-statistic is used here; $t_{0.025} = 2.012$
[b]t-statistic is used here; $t_{0.025} = 2.001$
[c]t-statistic is used here, $t_{0.025} = 1.989$

Table 9: r^2 regression values for peel force versus tread wear, 95% confidence intervals for slope of linear fit.

Category	r^2 linear-fit	Slope 95% CI	exponential-fit
Decatur N ATX	0.3131	-0.198±0.407	0.3000
Decatur N AT	0.0025	0.031±0.466	0.0004
Wilson N ATX	0.0326	-0.063±0.625	0.0304
Wilson N AT	0.0899	0.178±0.566	0.0646
Joliette N ATX	0.7563	-0.580±1.001	0.7378
Joliette N AT	0.0860	-0.178±0.409	0.0770
Decatur S ATX	0.0487	0.133±0.237	0.0402
Decatur S AT	0.2694	-0.225±0.160	0.2731
Wilson S ATX	0.0023	-0.052±0.825	0.0050
Wilson S AT	0.0702	-0.119±0.214	0.0762
Joliette S ATX	0.0227	0.140±0.921	0.0185
Joliette S AT	0.2241	-0.308±0.403	0.2421

Table 10: Means and standard deviations for peel force by tire model and plant.

Category	Mean (N)	Std. Deviation
Southern ATX	63.0	19.9
Northern ATX	71.12	15.4
Southern AT	72.2	14.2
Northern AT	78.31	12.6
Decatur South	58.31	11.0
Decatur North	65.13	9.59
Wilson South	77.57	16.9
Wilson North	82.17	11.1
Joliette South	78.90	18.8
Joliette North	82.43	12.9

Table 11: Mean differences and confidence intervals for peel forces.

Comparisons	Mean Difference 95% CI	z-statistic
Southern ATX vs Northern ATX	8.16±11.2	1.45[a]
Southern AT vs Northern AT	6.13±5.78	2.08
Southern AT vs Southern ATX	9.22±6.78	2.67
Northern AT vs Northern ATX	7.19±8.60	1.69[b]
Decatur South vs Wilson and Joliette South	19.8±5.64	6.88
Decatur North vs Wilson and Joliette North	17.2±6.79	5.06[c]
Zero Tread Wear Decatur South vs Wilson and Joliette South	19.2±11.4	3.60[d]
Zero Tread Wear Decatur North vs Wilson and Joliette North	21.1±23.6	2.19[e]

[a]t-statistic is used here; $t_{0.025} = 2.0$; Wilcoxon ranksum test rejects the standard null hypothesis at $\alpha = 0.05$ with a $z = 2.250$.

[b]t-statistic is used here; $t_{0.025} = 2.0168$; Wilcoxon ranksum test does not reject the standard null hypothesis at $\alpha = 0.05$ with a $z = 1.81$.

[c]t-statistic is used here; $t_{0.025} = 2.0168$; Wilcoxon ranksum test rejects the standard null hypothesis at $\alpha = 0.05$ with a $z = 4.27$.

[d]t-statistic is used here; $t_{0.025} = 2.131$

[e]t-statistic is used here; $t_{0.025} = 2.447$

Table 12: Peel force means converted to critical energy release rate by plant and model.

Category	Mean (kJ/ m^2)
Southern ATX	4.65
Northern ATX	5.06
Southern AT	5.12
Northern AT	5.41
Decatur South	4.40
Decatur North	4.76
Wilson South	5.37
Wilson North	5.58
Joliette South	5.43
Joliette North	5.59

Table 13: Percent of tires that showed belt edge cracking at either of the two circumferential locations examined and the total number of tires examined in this part of the study.

Category	Detection rate (%)	Sample size
Decatur South	26.0	172
Decatur North	4.6	152
Wilson South	48.0	50
Wilson North	16.0	31
Joliette South	61.0	46
Joliette North	23.0	31

Table 14: r^2 regression values for 100% modulus versus lubricant percentage and 95% confidence intervals for slope of linear fit.

Category	r^2 linear-fit	Slope 95% CI
Decatur J2917 new	0.984	0.246±0.043
Decatur J2917 aged	0.467	0.291±0.432
Wilson J2917 new	0.700	0.160±0.145
Wilson J2917 aged	0.260	0.217±0.509
Decatur J2757 new	0.630	0.149±0.158
Decatur J2757 aged	0.597	0.269±0.306
Wilson J2757 new	0.032	-0.034±0.261
Wilson J2757 aged	0.030	0.069±0.544

Table 15: r^2 regression values for ring toughness versus lubricant percentage and 95% confidence intervals for slope of linear fit.

Category	r^2 linear-fit	Slope 95% CI
Decatur J2917 new	0.374	-259.371±465.935
Decatur J2917 aged	0.274	74.229±167.579
Wilson J2917 new	0.291	-443.371±961.136
Wilson J2917 aged	0.101	44.857±186.203
Decatur J2757 new	0.522	-745.029±990.146
Decatur J2757 aged	0.006	-23.600±410.028
Wilson J2757 new	0.227	-176.171±450.713
Wilson J2757 aged	0.389	222.514±387.161

Table 16: r^2 regression values for one inch adhesion test versus lubricant percentage and 95% confidence intervals for slope of linear fit.

Category	r^2 linear-fit	Slope 95% CI
Decatur J2917 new	0.835	-6.448±3.982
Decatur J2917 aged	0.507	-2.450±3.353
Wilson J2917 new	0.764	-6.750±5.209
Wilson J2917 aged	0.288	-2.068±4.512
Decatur J2757 new	0.659	-4.283±4.279
Decatur J2757 aged	0.671	-3.136±3.046
Wilson J2757 new	0.000	0.040±6.649
Wilson J2757 aged	0.046	-0.503±3.188

B   Figures

Figure 1: Belt edge crack example from a steel belted radial tire.
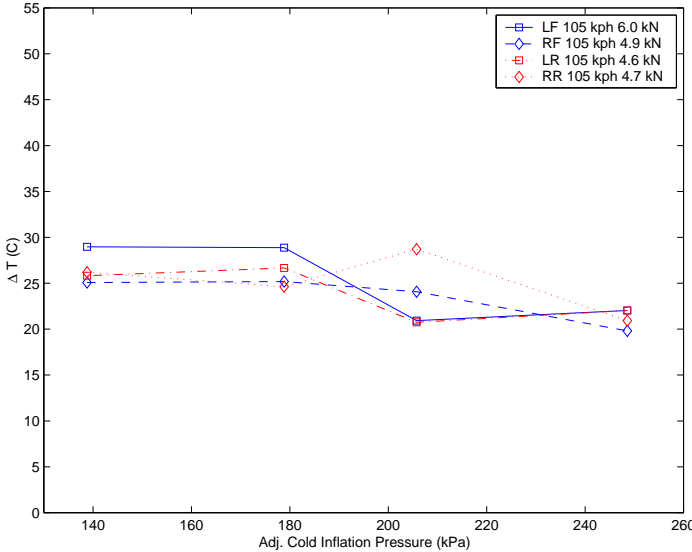
Figure 2: Thermal increment at belt edge versus cold adjusted inflation pressure at 105 kph for unloaded vehicle.
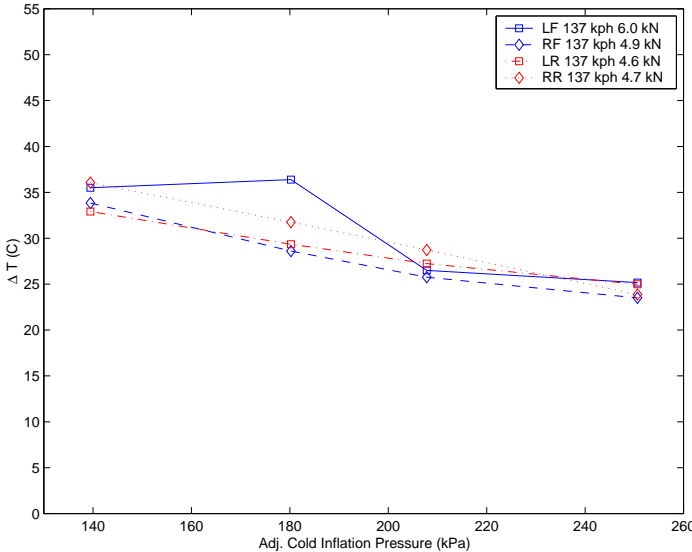
Figure 3: Thermal increment at belt edge versus cold adjusted inflation pressure at 137 kph for unloaded vehicle.
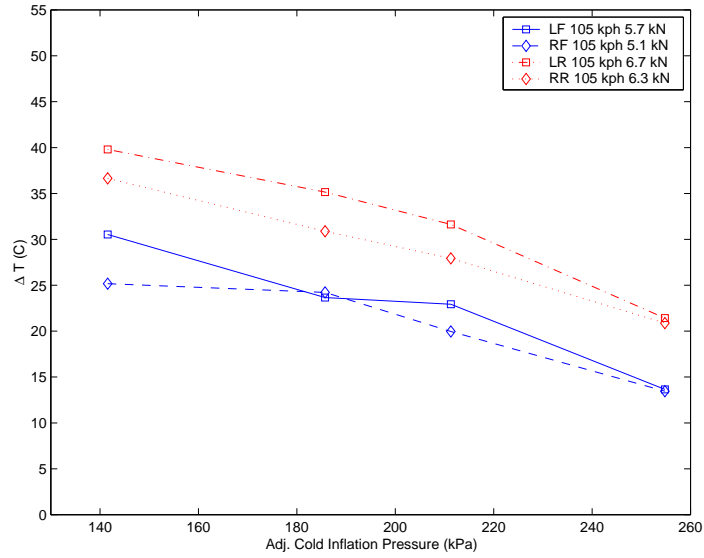
Figure 4: Thermal increment at belt edge versus cold adjusted inflation pressure at 105 kph for RGAWR loaded vehicle.
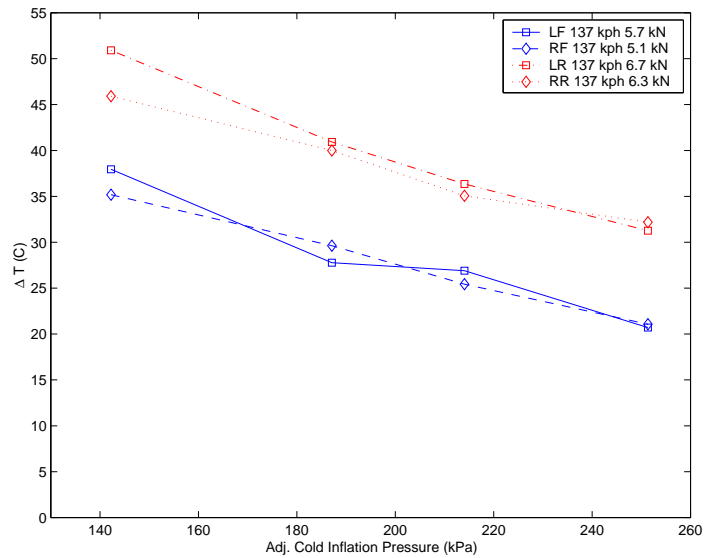
Figure 5: Thermal increment at belt edge versus cold adjusted inflation pressure at 137 kph for RGAWR loaded vehicle.

Figure 6: Close-up view of load cell affixed to tire.

Figure 7: Side view of Ford Explorer with load cells attached.
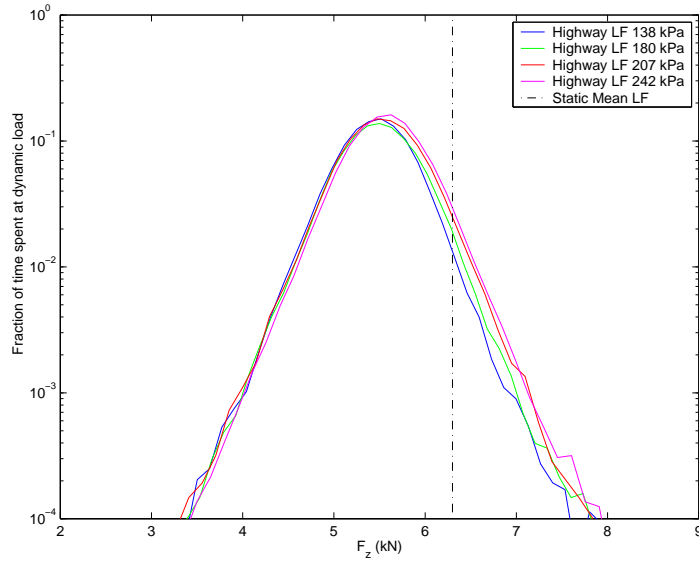
Figure 8: Dynamic load histogram for vertical forces applied by Explorer to left front tire at the Ranger RGAWR condition. Vertical line indicates static mean load.
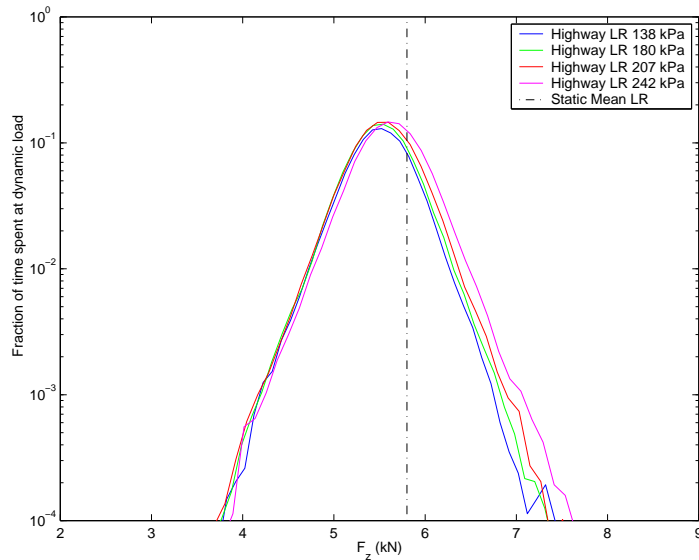
Figure 9: Dynamic load histogram for vertical forces applied by Explorer to left rear tire at the Ranger RGAWR condition. Vertical line indicates static mean load.
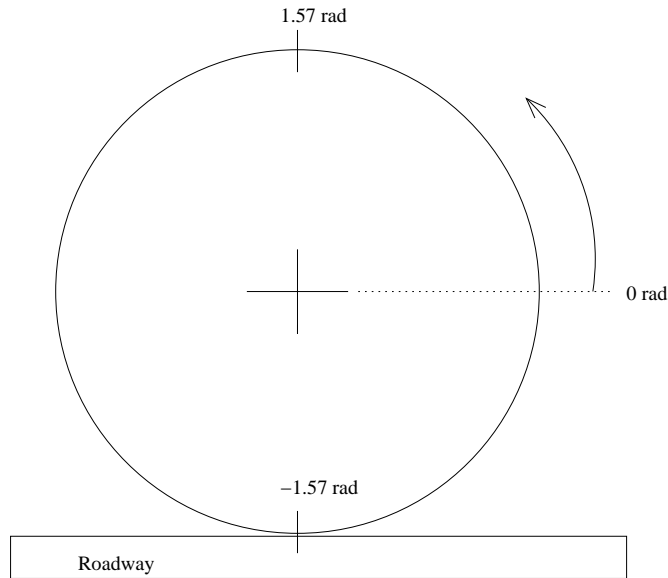
Figure 10: Angular position is measured counter-clockwise from the horizontal. Thus $-\pi/2$ denotes the center of the footprint and $\pi/2$ the top of the tire.
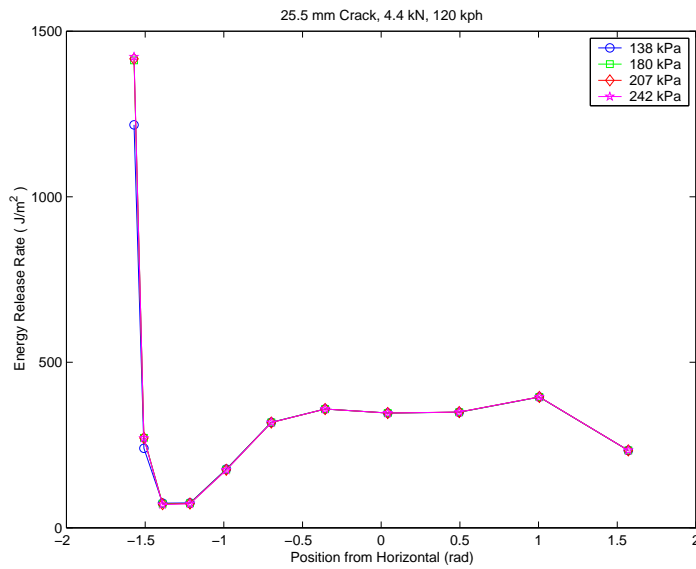
Figure 11: Energy release rate as a function of angular position from the horizontal for a 25.5 mm crack at 120 kph under a 4.4 kN load.
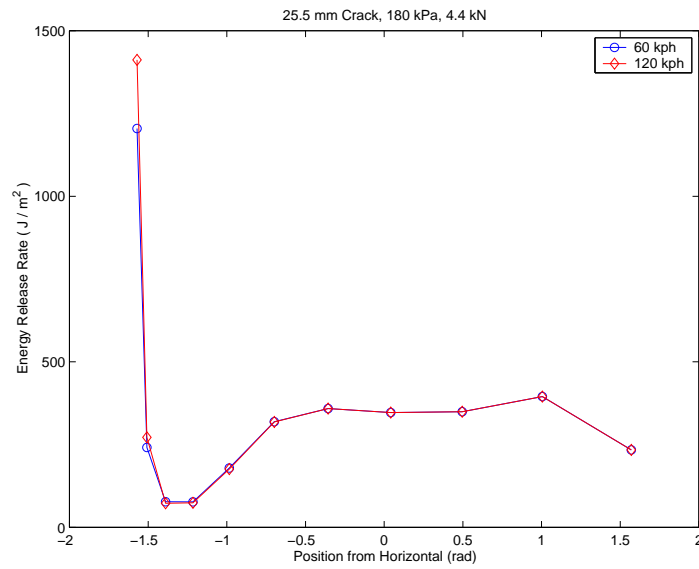
Figure 12: Energy release rate as a function of angular position from the horizontal for a 25.5 mm crack at an inflation pressure of 180 kPa and a 4.4 kN load.
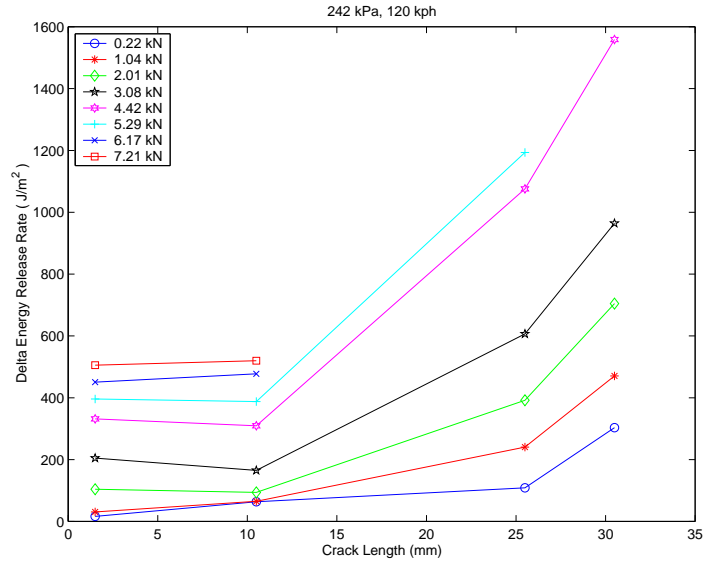
Figure 13: Energy release rate increments per revolution as a function of crack length indexed by vehicle tire load at an inflation pressure of 242 kPa and 120 kph.
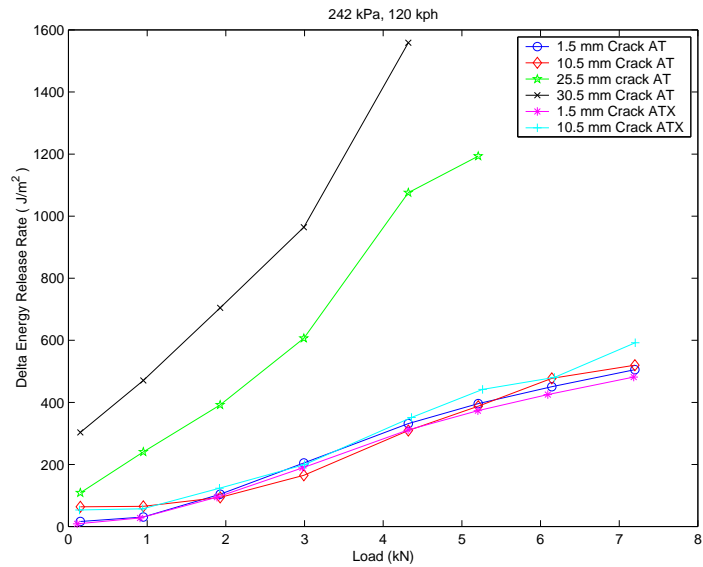
Figure 14: Energy release rate increments per revolution as a function of load indexed by crack length at an inflation pressure of 242 kPa and 120 kph.
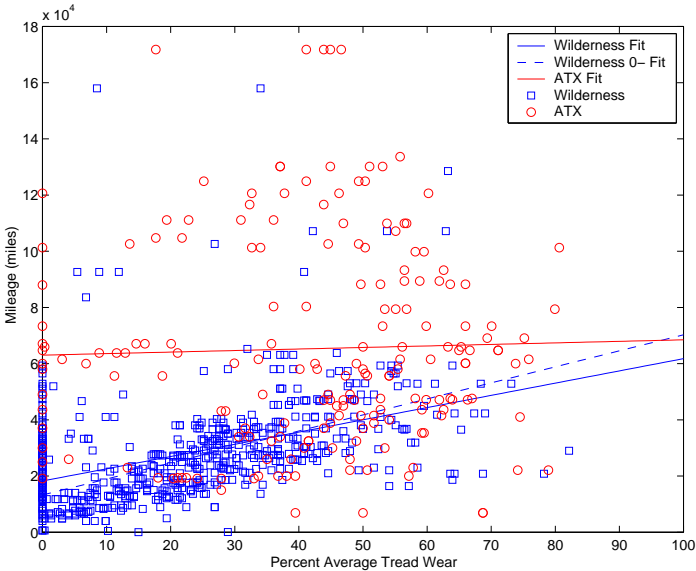
Figure 15: Self reported mileage versus average tread wear
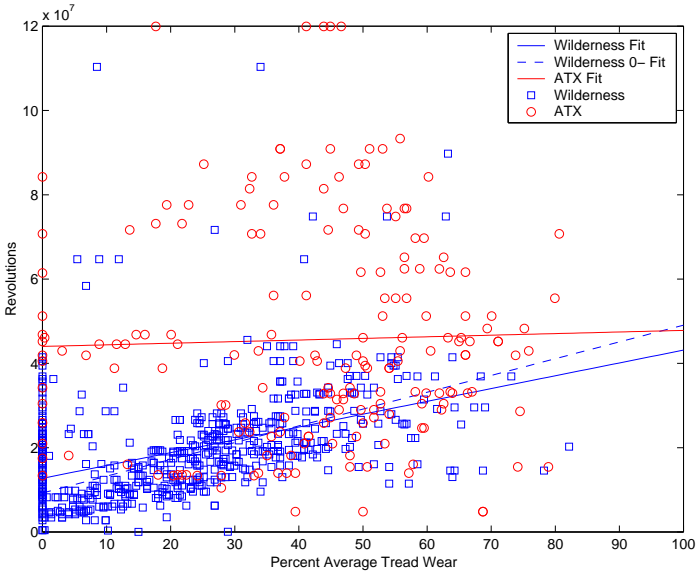
Figure 16: Tire revolutions based on self-reported mileage versus average tread wear
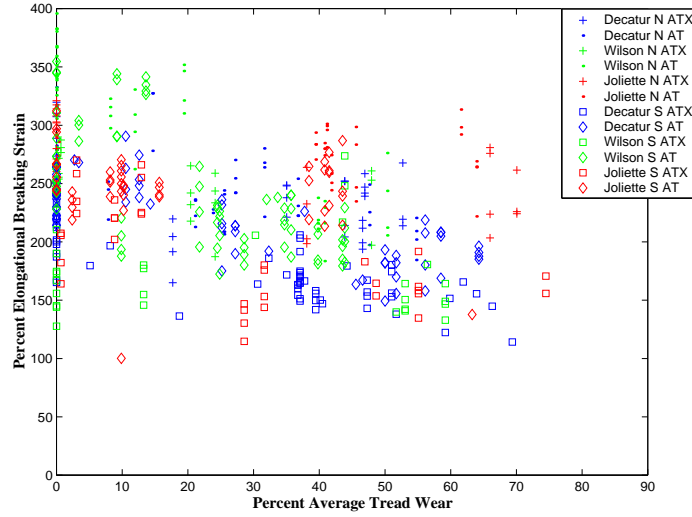
Figure 17: Wedge compound ductility measure from returned tires sorted by tire model, production plant, and usage latitude.
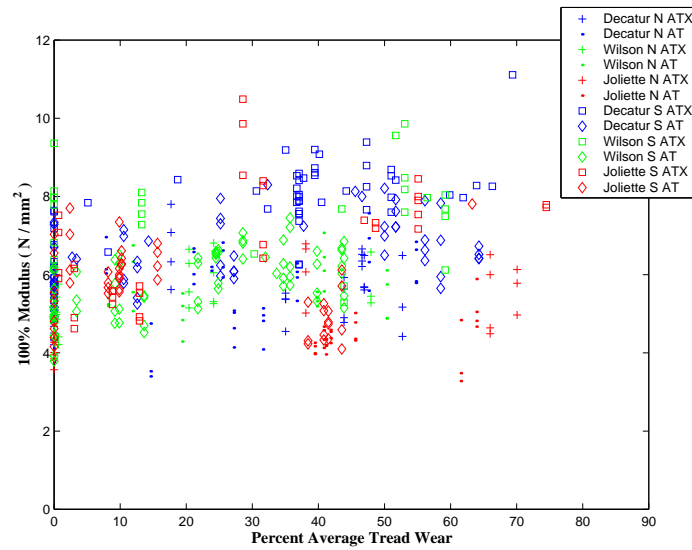
Figure 18: Wedge compound 100% modulus from returned tires sorted by tire model, production plant, and usage latitude.
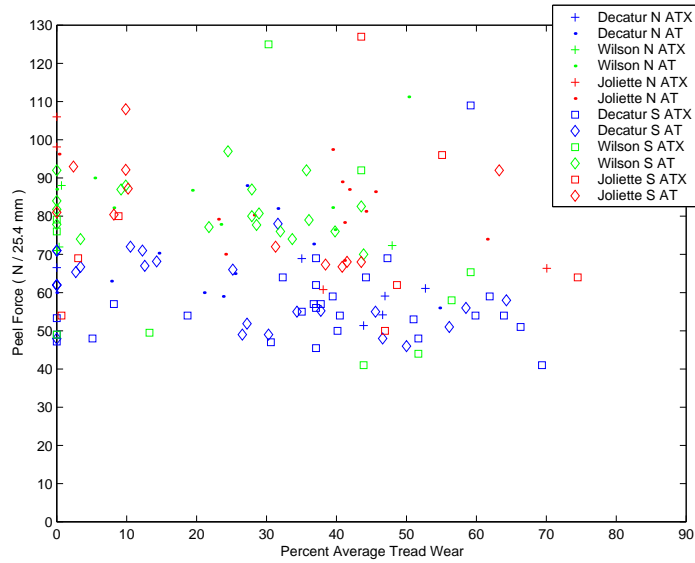
Figure 19: Belt package peel forces from returned tires sorted by tire model, production plant, and usage latitude.

Figure 20: Peel test surface for F44 manufactured in Decatur. Distance between reflective peeks of steel cords is approximately 1.4 mm.

Figure 21: Peel test surface for F89 manufactured in Wilson. Distance between reflective peeks of steel cords is approximately 1.4 mm.
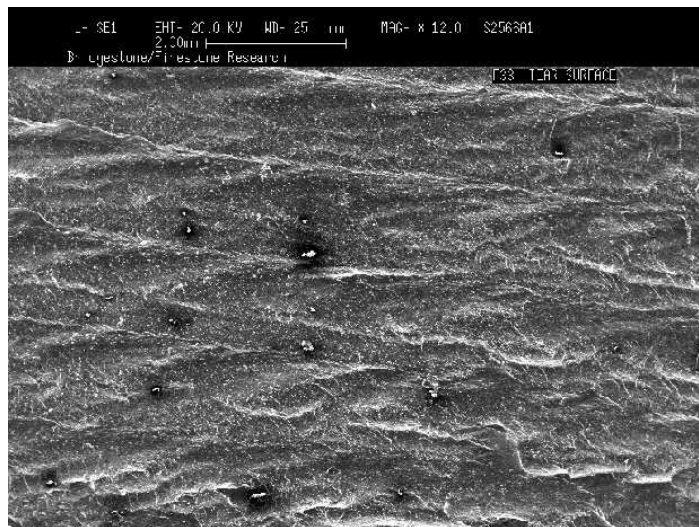
Figure 22: Peel test surface for F33 manufactured in Decatur. See micrograph legend for 2mm scale bar.
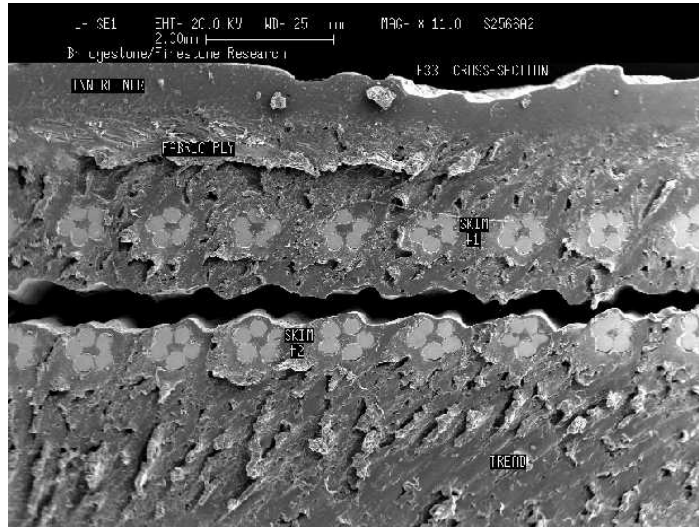
Figure 23: Peel test cross-section for F33 manufactured in Decatur. See micrograph legend for 2mm scale bar.
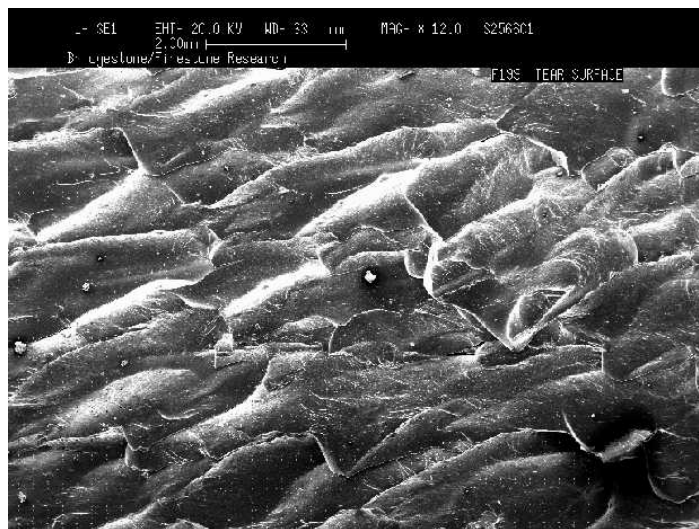
Figure 24: Peel test surface for F199 manufactured in Wilson. See micrograph legend for 2mm scale bar.
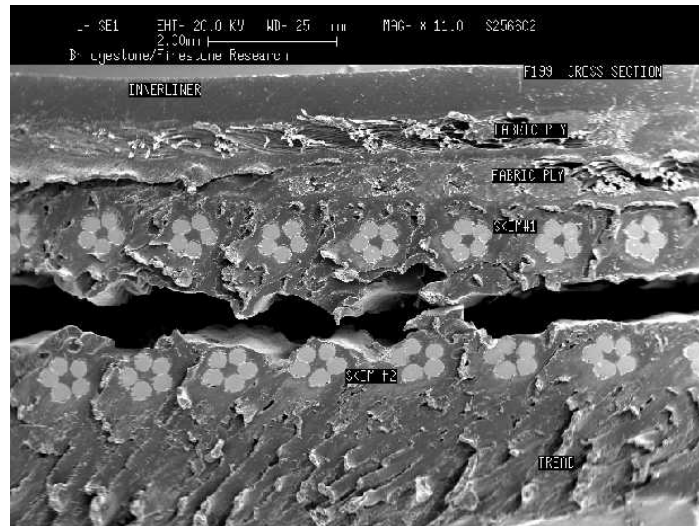
Figure 25: Peel test cross-section for F199 manufactured in Wilson. See micrograph legend for 2mm scale bar.
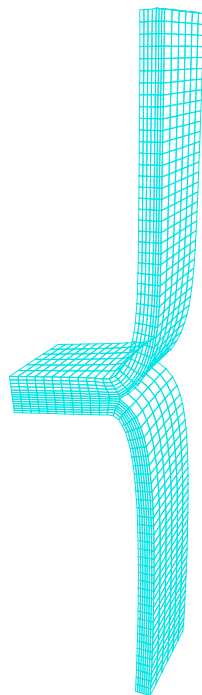
Figure 26: Deformed mesh of a peel test simulation.
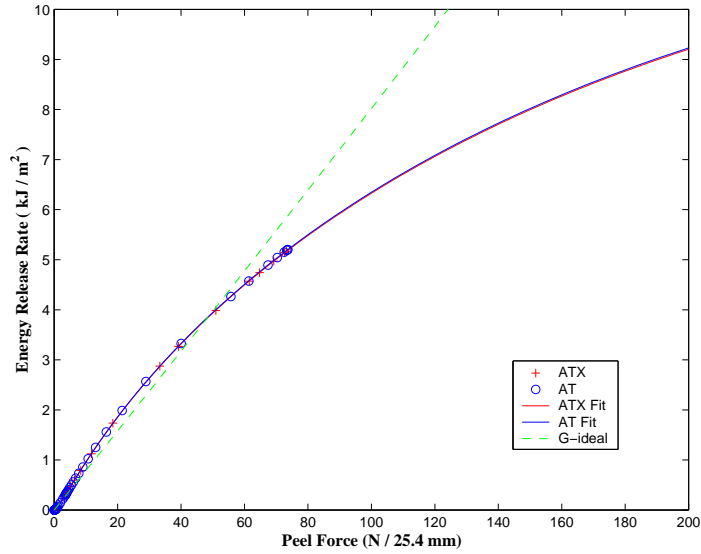
Figure 27: Critical energy release rate versus peel force estimated using finite element analysis. Regression fits shown utilize fractional exponent series. G-ideal corresponds to Eq. (3).
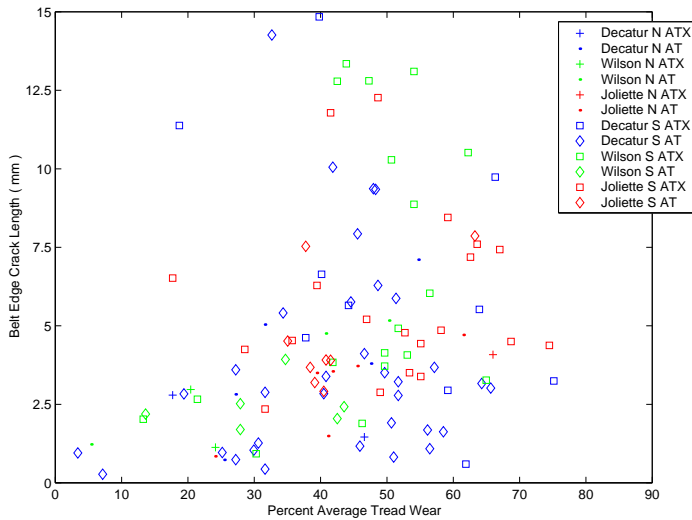
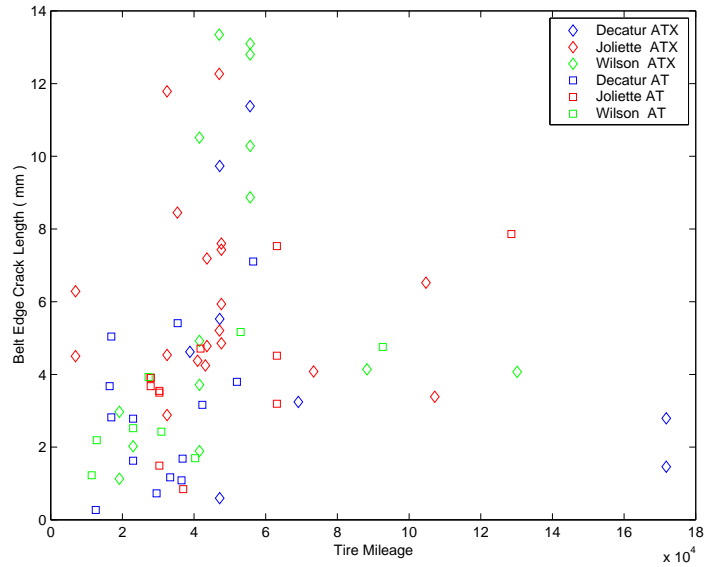Figure 28: Average belt edge crack lengths versus tread wear from returned tires.

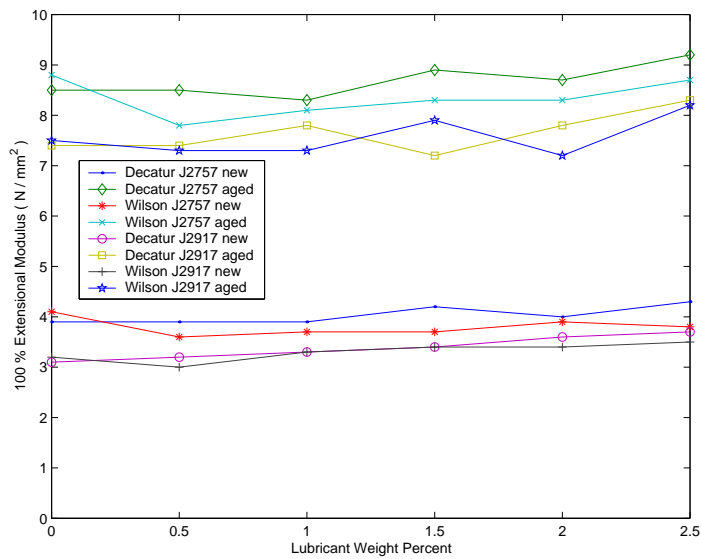Figure 29: Average belt edge crack lengths versus mileage from returned tires.

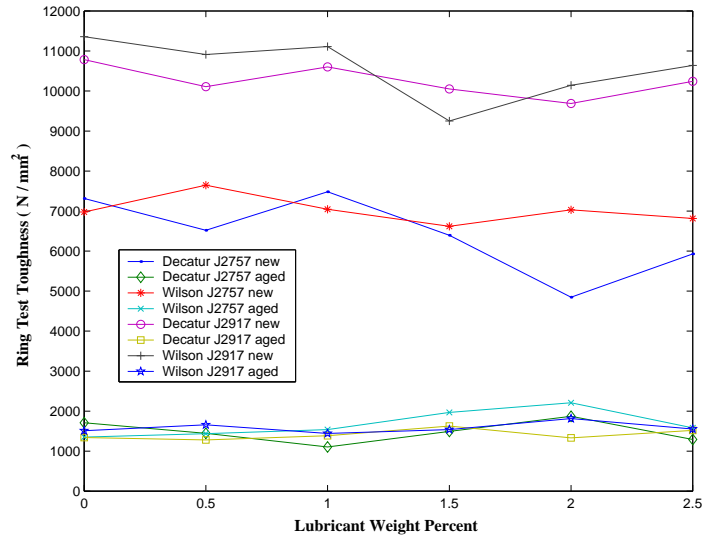Figure 30: 100% extensional modulus as a function of lubricant amount.

Figure 31: Ring toughness as a function of lubricant amount.

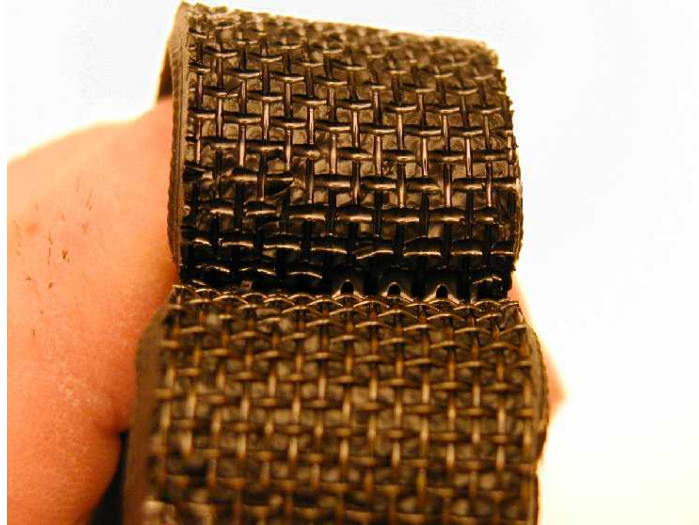Figure 32: One inch adhesion strip test.

Figure 33: Close-up view of the failure front in the one inch adhesion strip test.
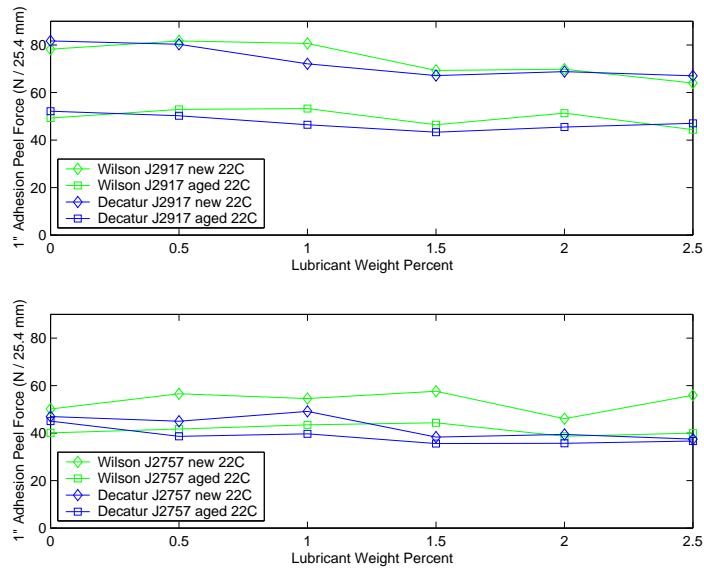

Figure 34: One inch adhesion peel test results versus lubricant weight percentage.
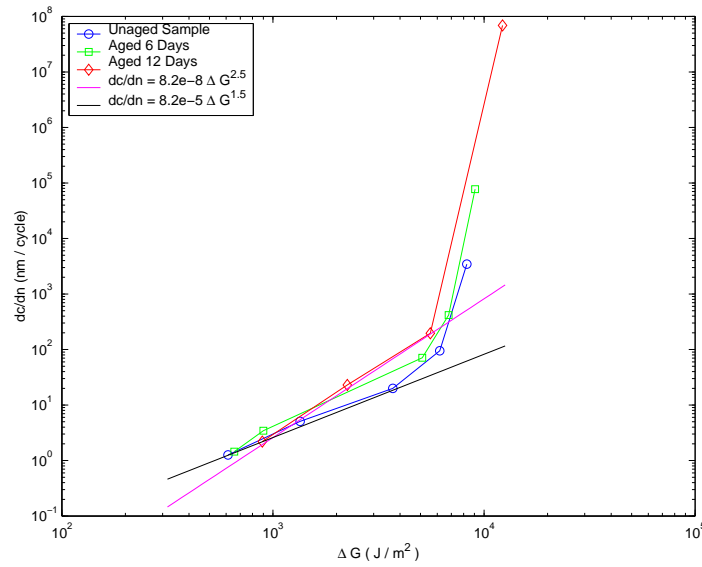
Figure 35: Cut growth curves for J2757 in the unaged, 6 day aged, and 8 day aged conditions.

C   Glossary

Crack tip driving force is a synonym for energy release rate.

Critical energy release rate is a material property that describes the maximum energy release rate a material can support before a given crack will begin to propagate in a catastrophic manner. At energy release rates below the critical value, cracks will only propagate in an incremental fashion. Note that natural rubber does not display appreciable time-dependent fracture as is seen in synthetic rubbers.

Energy release rate is a measure of the forces that are trying to increase the length of a crack.

Footprint is the region where the tire contacts the roadway.

Null hypothesis normally refers to a hypothetical statement that one is interested in proving false. A statistical test is applied to the hypothesis to ensure that it is false to within a certain probability; in standard hypothesis testing this probability is usually taken as 95%. For the purposes of this report, the null hypothesis is the assumption that the populations being compared are the same. Thus rejection of the null hypothesis indicates that the sample populations are different.

r^2 is a measure of the percent of variance of an outcome variable that can be explained by the variance of a predictor variable.

RGAWR is the rear gross axle weight rating.

t-statistic: This is a measure used in hypothesis testing when sample sizes are small (less than 30). It is similar in nature to the z-statistic but the critical values that correspond to a particular level of certainty change with sample size. Listed in the footnotes of the tables that use t-statistics are the values that correspond to a level of certainty of 95% in favor of rejecting the null hypothesis. Higher values of the t-statistic indicate even greater certainty in rejecting the null hypothesis.

Tearing energy is a synonym for energy release rate that is commonly used in the rubber industry.

Wilcoxon is a statistical test to determine if two distributions differ from each other.

z-statistic: This is a measure used in hypothesis testing when sample sizes are large (greater than 30). When testing a null hypothesis a value of 1.96 roughly indicates a level of certainty of 95% in favor of rejecting the null hypothesis. Higher values of the z-statistic indicate even greater certainty in rejecting the null hypothesis.

95% confidence intervals denote the interval within which a given variable will be found with 95% certainty.